LANDSLIDE TSUNAMI HAZARD ALONG THE UPPER U.S. EAST COAST: EFFECTS OF SLIDE RHEOLOGY AND BOTTOM FRICTION

BY

LAUREN SCHAMBACH[1], STEPHAN T. GRILLI[1],

JAMES T. KIRBY[2], AND FENGYAN SHI[2]

[1] DEPARTMENT OF OCEAN ENGINEERING, UNIVERSITY OF RHODE ISLAND

[2] CENTER FOR APPLIED COASTAL RESEARCH, DEPARTMENT OF CIVIL AND ENVIRONMENTAL ENGINEERING, UNIVERSITY OF DELAWARE

RESEARCH REPORT NO. CACR-17-04
OCTOBER 2017

CENTER FOR APPLIED COASTAL RESEARCH

University of Delaware
Newark, Delaware 19716

Abstract

We perform numerical simulations to assess tsunami hazard along the upper US East Coast (USEC; From Virginia to Cape Cod, MA), caused by Submarine Mass Failures (SMFs) triggered on the continental shelf slope, considering the effect of SMF rheology, i.e., whether the SMFs behave as rigid slumps or deforming slides. We simulate tsunami generation using the three-dimensional non-hydrostatic model NHWAVE. For rigid slumps, the geometry and law of motion are specified as bottom boundary conditions and for deforming slides SMF motion and deformation are modeled in a depth-integrated bottom layer of dense Newtonian fluid, fully coupled to the overlying fluid motion. Once the SMFs are no-longer tsunamigenic, we continue simulating tsunami propagation using the two-dimensional fully nonlinear and dispersive long wave model FUNWAVE-TVD. For the onshore tsunami propagation, we use nested grids of increasingly fine resolution towards shore and apply a one-way coupling methodology. As in earlier work, we only simulate probable maximum tsunamis generated by Currituck SMF proxies, i.e., SMFs having the same volume and footprint as the historical Currituck slide complex, the largest known on the USEC. These proxies are sited in four areas of the shelf break slope identified to have enough sediment accumulation to cause large failures. In tsunami generation simulations, we find that deforming slides have a slightly larger initial acceleration, but still generate a smaller tsunami than rigid slumps due to their spreading and thinning out during motion, which gradually makes them less tsunamigenic; by contrast, rigid slumps keep their specified shape during their pendulum-like motion. We compare the combined maximum envelope of surface elevation caused along the shore (5 m isobath) by these SMF tsunamis. Consistent with earlier work, we find that the bathymetry of the wide shelf strongly controls the magnitude of tsunami coastal inundation, as it induces wave focusing and defocusing effects. Additionally, tsunami propagation and refraction over the shelf, both north and south of each source area, causes non-trivial variations in surface elevation and coastal inundation. As a result, SMF tsunamis can cause a significant coastal impact far alongshore from their source area. Overall, tsunamis caused by rigid slumps are worst case scenarios (absolute maximum inundation about 11.5 m around Montauk, NY), providing up to 50% more inundation than for slides having a moderate level of deformation (viscosity set in the upper range of debris flows). Regarding minimum elevations at the coast, which affect power plant intakes, tsunamis from both types of SMFs are shown to be able to cause water withdrawal to the 5 m isobath or deeper. Finally, bottom friction effects are assessed by performing some simulations using two different Manning coefficients, one 50% larger than the other; with the increased friction, the largest tsunami inundations at the coast are reduced, in some cases, by up to 15%.

Contents

List of Figures

List of Tables

1 Introduction

This study was performed as part of tsunami hazard assessment work carried out since 2010 under the auspices of the US National Tsunami Hazard Mitigation Program (NTHMP). In this work, the authors developed tsunami inundation maps for the US East Coast (USEC), by modeling tsunami generation, propagation, and coastal impact for a series of extreme sources selected in the Atlantic Ocean basin (Grilli et al., 2010; Tehranirad et al., 2015; Grilli et al., 2017a), to trigger so-called Probable Maximum Tsunamis (PMTs). These inundation maps thus represent the envelope of maximum inundation resulting from the combined coastal impact of these tsunamis, without consideration of return periods (ECMAP, 2017; Tehranirad et al., 2014, 2015a,b,c,d,e). Tsunami generation and propagation were simulated using two-dimensional (2D) Boussinesq (Shi et al., 2012; Kirby et al., 2013) and three-dimensional (3D) non-hydrostatic (Ma et al., 2012) wave models, in a series of nested spherical and Cartesian grids of increasingly fine resolution towards the coast. These grids were built using commensurately accurate bathymetric and topographic data, the finer coastal grids typically having a 10-30 m resolution.

This work, as well as other earlier studies, showed that along the upper USEC the hazard is dominated by near-field tsunamis that could potentially be generated by large submarine mass failures (SMFs) (ten Brink et al., 2008, 2009a,b; Grilli et al., 2009; ten Brink et al., 2014; Grilli et al., 2015, 2017a,b). The moderate seismicity typical of the region would not be expected to cause significant near-field co-seismic tsunamis, but could trigger large SMFs, particularly where sediment accumulates over steep slopes on the continental shelf break, off of major estuaries. In fact, the largest earthquake ever measured in the USEC area, with a Mw 7.2 magnitude, was responsible for triggering the 1929 landslide tsunami off of the Grand Banks (Piper et al., 1999; Fine et al., 2005). With a maximum runup of 13 m, this tsunami caused widespread destruction of coastal communities and 28 casualties in Newfoundland. The SMF displaced over 100 km^3 of sediment, turning into a turbidity current that reached speeds of 17-28 m/s, breaking 12 underwater communication cables in the process. Confirming that the 1929 landslide was not an isolated event, ten Brink et al. (2014) mapped numerous paleo-SMFs on the US Atlantic continental shelf and margin, with the largest one being the Currituck slide complex (Locat et al., 2009), off of Chesapeake Bay (Fig. 1). If it had failed in present days, this paleo-SMF would have generated a destructive tsunami for the upper USEC (Geist et al., 2009; Grilli et al., 2015). Recent field work (Hill et al., 2017) has dated this old slide complex to 16-50Ka, but Chaytor (personal communication) indicates that its age is likely on the younger end of this range. Considering when this failure occurred, the sea level would have been much lower than in present days.

To assess SMF tsunami hazard along the USEC, Grilli et al. (2009) performed Monte Carlo Simulations (MCS) of SMFs triggered by seismicity along a series of transects defined perpendicular to the coastline. These were initially sited from southern New Jersey to Cape Cod, MA, but the study was later extended by Krauss (2011) to southern Florida, yielding a total of 91 transects for the entire USEC. In the MCS, thou-
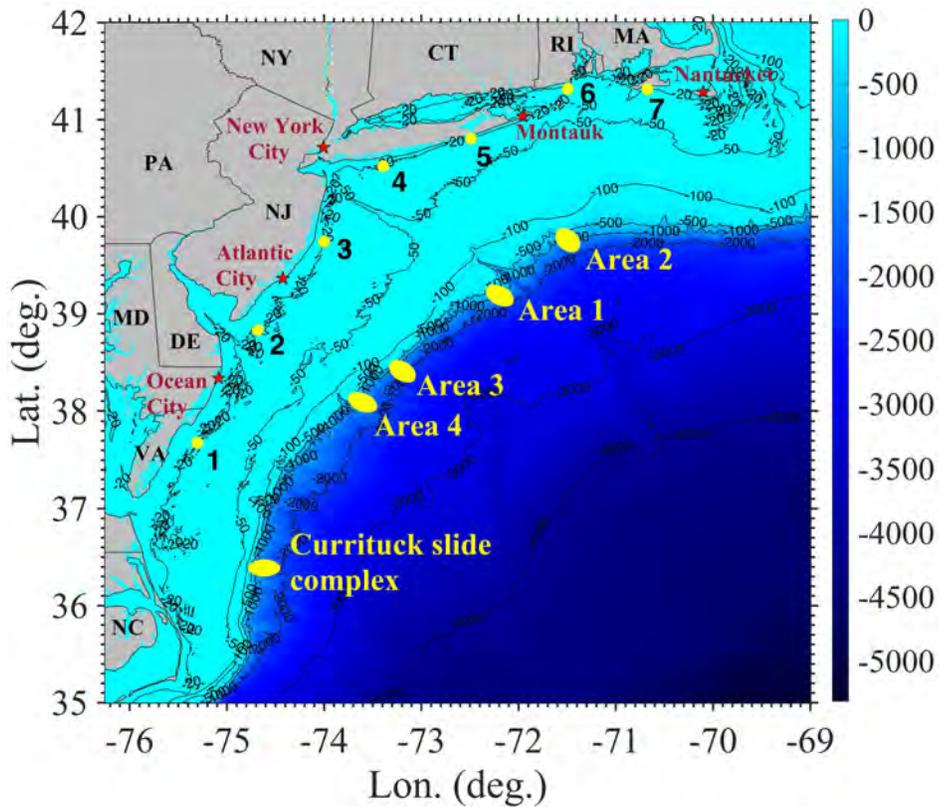
Figure 1: Geography of study area (with marked state limits and names, and names of a few cities (red stars) identified). Areas 1-4, identified by (Grilli et al., 2015) as having high potential for large tsunamigenic SMFs, and the location of the historical Currituck slide complex are marked by yellow ellipses. Numerical gage stations 1-7 (20 m depth) are marked by yellow bullets. The color scale and bathymetric contours show depth in meters.

sands of potential SMFs were generated along each transect, with associated random values of geometry, sediment properties, mechanism–slide or slump–, depth, and excess pore pressure, selected from assumed probability distributions and/or site specific field data. The selection of a failure mechanism was entirely based on the sediment nature, with slumps being associated with cohesive clay-type sediments and slides with non- (or less-)cohesive silt-type sediments. Local seismicity was randomly selected from USGS data (i.e., from curve fitted probability distributions of peak horizontal acceleration). Standard slope stability analyses were performed for each potential failure and, for unstable cases, tsunami generation and runup were calculated based on semi-empirical equations developed by Watts et al. (2005). At the time, it was not thought possible to apply actual tsunami generation and propagation models to such a large number of cases. These results allowed estimating the 100 and 500 year return period SMF tsunami runups along the entire USEC, which predicted a 500 year runup of up to 5-6 m north of Virginia and a significantly reduced runup south of it. Eggeling (2012) used these results as guidance to carry out geophysical and geotechnical analyses on seafloor data collected in regions facing segments of the coast with the largest runup. This led to selecting four areas (Fig. 1) where, given sufficient seismicity, large tsunamigenic SMFs could be expected to occur. These areas typically had a large bottom slope and a sediment thickness sufficient to make a large failure possible. More detailed slope stability analyses, performed using the model SLIDE (SLIDE, 2017), yielded low factors of safety in these areas, confirming the high likelihood of failure.

As part of their NTHMP inundation mapping work, which was based on PMTs, Grilli et al. (2015) modeled SMF tsunami hazard along the upper USEC by simulating tsunami generation from large SMFs sited in Areas 1-4 identified by Eggeling (2012) (Fig. 1), using the 3D non-hydrostatic model NHWAVE (Ma et al., 2012). In the absence of detailed site specific information, these were parameterized using the characteristics of the largest known historical failure in the region, i.e., the Currituck slide complex (Fig. 1); for this reason they are referred to as "Currituck SMF proxy" sources. The Currituck slide complex has been extensively studied from geological and slide triggering points of views (e.g., Locat et al. (2009), and references herein). Tsunami generation from a reconstituted Currituck SMF was first modeled by Geist et al. (2009), using a simplified SMF tsunami generation model. To maximize tsunami generation, Grilli et al. (2015) considered that each Currituck SMF proxy was made of a single large failure, with a volume in the 128-165 km^3 range estimated for the whole Currituck slide complex by Locat et al. (2009). They assumed that each SMF failed as a rigid slump, which based on earlier work was expected to maximize tsunami generation and coastal impact (Grilli and Watts, 2005). In the slump law of motion, they used the maximum velocity of the SMF center of mass estimated by Locat et al. (2009) ($\simeq 35$ m/s). Once the slumps had stopped moving and tsunami generation was complete, simulations of tsunami propagation and coastal impact were performed using the 2D Boussinesq model FUNWAVE-TVD (Shi et al., 2012) (referred to hereafter as FTVD), in a series of nested grids. Results of these simulations were used to develop the NTHMP tsunami inundation maps currently released for the upper USEC region

3

(ECMAP, 2017).

More recently, Grilli et al. (2017b) investigated the effects of SMF kinematics and rheology on tsunami hazard, using the newer two-layer version of NHWAVE (Kirby et al., 2016), referred to here as NHWAVED (for NHWAVE deforming). In this model, deforming slides are modeled as a dense Newtonian fluid, in a depth-integrated bottom layer, and the coupled upper water layer flow is simulated with the standard multi-σ-layers NHWAVE model. Grilli et al. (2017b) first simulated the historical Currituck SMF with this model, to estimate relevant values of slide viscosity ν_s and bottom friction Manning coefficient, n (between slide and substrate). This was done by finding values that yielded a slide center of mass motion $S(t)$ similar to that Grilli et al. (2015) used in rigid slump simulations, and a maximum runout S_f similar to the slump, after a time of motion t_f. They inferred a fairly large viscosity ($\nu_s = 0.5$ m^2/s), which was then used to model the Currituck SMF proxy in Area 1 (Hudson River canyon) as a deforming slide. Comparing the computed maximum surface elevation nearshore (over the 5 m isobath) to that caused by the rigid slump, they found that, despite the high viscosity, due to the spreading-out of the deforming slide during its motion, the SMF acceleration and related maximum tsunami elevations were reduced as compared to the rigid slump. Also because the deforming slide flowed on its own (rather than having its motion prescribed), it followed the steepest bottom slope and the generated tsunami ended up being more asymmetrical than for the slump. This latter feature affects where maximum tsunami impact occurs along the coast, and hence the level of hazard. They concluded that modeling tsunami hazard by considering that all the SMF fail as rigid slumps was likely too conservative, although the opposite could be true in some site specific situations. Hence, it should be more realistic (i.e., in better agreement with field observations in the region) to consider tsunami generation from deforming slides, even if only a moderate level of deformation (i.e., a high viscosity) is considered.

In light of these conclusions, in this paper, we follow a methodology similar to that of Grilli et al. (2017b) to more realistically assess landslide tsunami hazard along the upper USEC (from Virginia to Massachusetts), by modeling tsunami generation and propagation from Currituck SMF proxies sited in Areas 1-4 (Fig, 1), failing as deforming slides. For comparison, since we use higher-resolution computational grids, we also recompute tsunami generation and propagation for the same SMFs failing as rigid slumps (as in Grilli et al. (2015)). Additionally, since earlier work indicated a significant effect of bottom friction on tsunami propagation for wide shelves (Geist et al., 2009; Grilli et al., 2015; Tehranirad et al., 2015), unlike Grilli et al. (2015) who used a constant bottom friction coefficient value $C_d = 0.0025$ in their FTVD simulations, we use a depth-dependent value of C_d, modeled with Manning's formula, as a function of Manning's coefficient n. We use $n = 0.025$ s^2/m$^{2/3}$ throughout, but also compare the resulting tsunami coastal impact for $n = 0.025$ and 0.0375, in one of the most impacted areas of the USEC, in northern New Jersey and western Long Island, NY. Results are provided as instantaneous surface elevations maps, time series of surface elevation at numerical wave gages, and envelopes of tsunami surface elevations, for the combination

of the 4 SMFs. This allows assessing tsunami hazard from extreme SMFs, along the USEC from Virginia to Cape Cod, MA.

In the following, in Section 2, we summarize the modeling methodology, in Section 3, we present simulations of SMF tsunami generation with NHWAVE and in Section 4, of SMF tsunami propagation and coastal impact with FTVD; this is followed by a discussion with conclusions in Section 5.

2   Modeling methodology

2.1   Numerical models

Tsunami generation by SMFs is modeled using the 3D non-hydrostatic model NHWAVE (Ma et al., 2012), when considering rigid SMFs of specified center of mass motion, and the newer two-layer NHWAVED model (Kirby et al., 2016), when simulating deforming SMFs as a dense Newtonian fluid. In both cases, the model uses a horizontal Cartesian grid of resolution $(\Delta x, \Delta y)$ and a boundary fitted σ-coordinate grid, with N_σ layers in the vertical direction. Once the tsunami is fully generated (this will be discussed below), the modeling of wave propagation is pursued with the 2D fully nonlinear and dispersive long wave Boussinesq model FTVD; because only regional grids of small geographic extent are considered, the Cartesian coordinate version of FTVD was used(Shi et al., 2012). As in earlier work, FTVD simulations are performed by one-way coupling in a series of nested grids of increasingly fine resolution (see, e.g., Grilli et al. (2013, 2015, 2017a,b); Tappin et al. (2014); Shelby et al. (2016), for details and examples of this approach).

Both NHWAVE(D) and FTVD are non-hydrostatic, i.e., dispersive, wave models. Numerous earlier works have clearly identified the importance of including frequency dispersion effects in the modeling of SMF tsunami generation and propagation, essentially due to the typically smaller wavelength to depth ratio of the generated waves (see, e.g.,Grilli and Watts (1999, 2005); Tappin et al. (2008); Ma et al. (2012)) In particular, Tappin et al. (2008) and Ma et al. (2012) showed that turning off dispersion in their landslide tsunami simulations caused large errors on the shape and kinematics of the generated waves. Additionally, without dispersion in the models the generated wave trains lacked in constructive-destructive wave-wave interactions during propagation, leading to significant errors in wave height and steepness when reaching shallow water; the generated wave trains also typically lacked the oscillatory (dispersive) bores and tails observed for landslide tsunamis, experimentally (see references listed in Grilli et al. (2017b)), in the field (e.g., Tappin et al. (2014)), or numerically (e.g., Tappin et al. (2008); Løvholt et al. (2008); Abadie et al. (2012); Grilli et al. (2015); Tehranirad et al. (2015)), and were limited to one or two leading waves.

To specify the geometry and kinematics of rigid slumps, we follow the methodology detailed in Grilli et al. (2015), in which these are specified as bottom boundary conditions in NHWAVE (see also Grilli and Watts (2005); Watts et al. (2005); Enet and

Grilli (2007)). In addition to the references, a summary of this methodology is given in Appendix A. For deforming slides, as in Grilli et al. (2017b), we use NHWAVED where the SMFs are modeled as a layer of dense fluid, couple, along the SMF-water interface with an upper water layer represented by σ-layers and a free surface, as in NHWAVE. In the bottom layer, SMF equations of mass and momentum conservation are depth-integrated, similar to those obtained in a long wave generation model, and include both volumetric (i.e., viscous) and bottom friction dissipation terms. The geometry of both rigid and deforming SMFs is modeled as an initial sediment mound of quasi-Gaussian cross-sections and elliptical footprint over the slope (see, Enet and Grilli (2007); Grilli et al. (2015), and Appendix A Eqs. (1) to (3), for details).

For rigid slumps, tsunami generation ends when the SMF reaches its maximum runout and stops moving. Deforming slides, however, keep moving (i.e., flowing) for a much longer time down the continental slope. Hence, at the time selected to continue simulations with FTVD (here 20 min), deforming slides are still moving and hence a time dependent bottom boundary condition is specified on NHWAVED's bottom. Grilli et al. (2017b) observed, in their coarser grid simulations of deforming slides in Area 1, that when initializing FTVD using results computed in NHWAVED with this non-homegeneous bottom boundary condition, spurious (rebound) waves were generated offshore in FTVD. They circumvented this problem by filtering out velocities over the location of the slide, before initializing FTVD. Because the slide was far offshore at this time and no-longer tsunamigenic, this did not affect simulations of the tsunami onshore propagation. A similar method is used in the present simulations.

2.2 Computational grids

SMF tsunami generation is computed with NHWAVE(D) in Areas 1-4, in four distinct Cartesian grids centered around each SMF (Fig. 2a). Each grid has a $\Delta x = \Delta y = 500$ m horizontal resolution, $N_\sigma = 5$ σ-layers in the vertical direction, and covers a 500 by 500 km footprint (i.e., each has 1,000 by 1,000 cells; see SW corner coordinates in Table 1). NHWAVE(D)'s Cartesian grid coordinates and bathymetry are constructed by mapping, with the projection center in each grid specified at each SMF initial location (x_0, y_0) (Table 1). NHWAVE(D)'s grids are all embedded within the $\Delta x = \Delta y = 500$ m Cartesian grid G0 that is the first-level (or base) grid used in FTVD to continue simulations of tsunami propagation; this grid covers an 800 km by 800 km area and, hence, has 1,600 by 1,600 cells (Fig. 2; see details in Table 2). After tsunami waves have been generated with NHWAVE(D), the surface elevation, bottom bathymetry, and (u, v) horizontal velocities (at the required depth of $0.531h$ for FTVD; Shi et al. (2012)), computed for each case, are interpolated onto FTVD's grid G0. These initial conditions are used to continue simulations of tsunami wave propagation to shore for each SMF, in grid G0 and then in 7 nested Cartesian grids of resolution $\Delta x = \Delta y = 120$ m (Fig. 2b; Table 2). To eliminate reflection at its offshore boundary, 125 km thick sponge layers are specified on both the eastern and southern boundaries of grid G0.

The bathymetry used in each grid is interpolated from the 3-arc second ($\simeq 90$
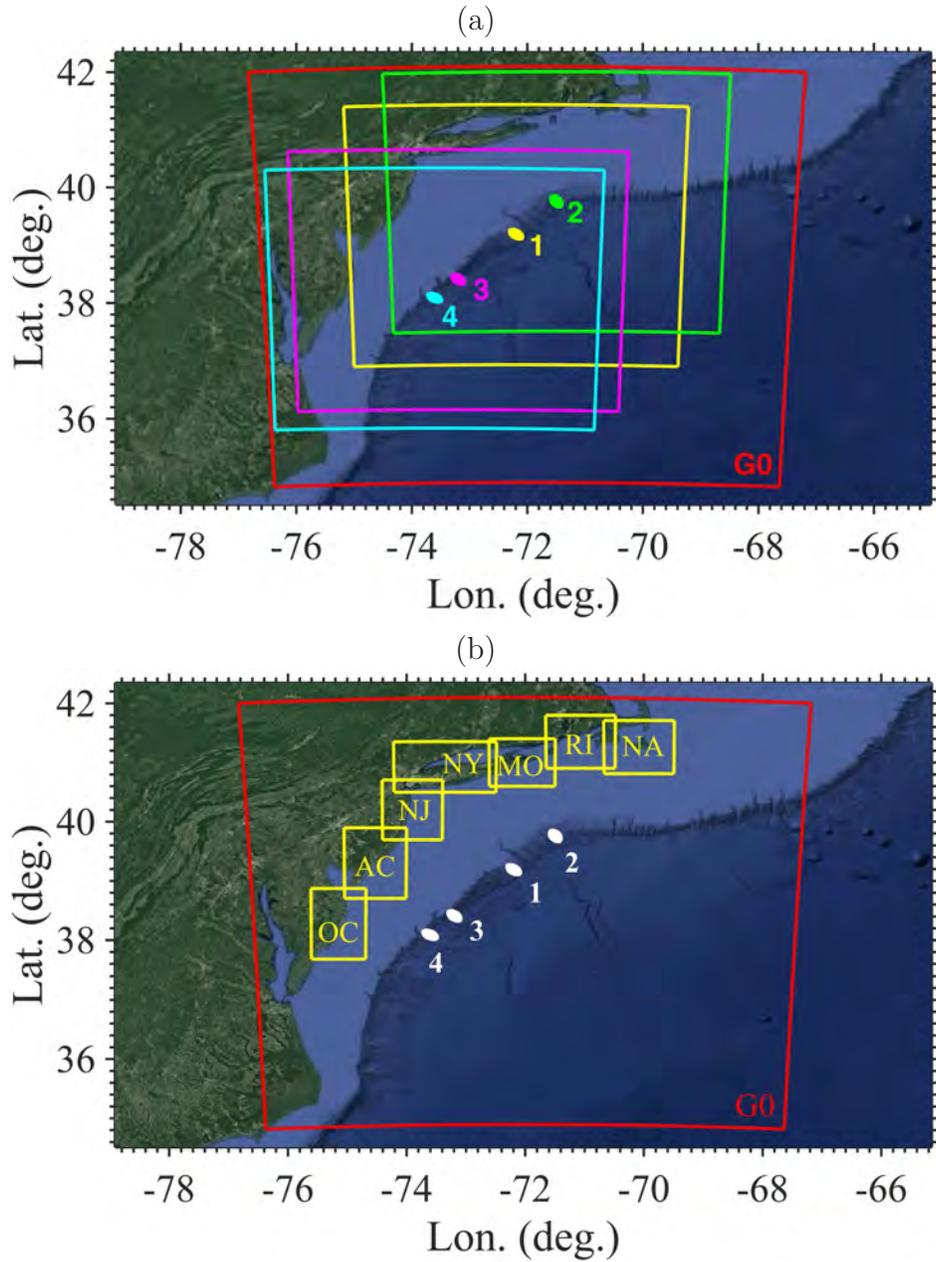
Figure 2: Horizontal footprints of computational grids used with: (a) NHWAVE: 4 color coded $\Delta x = \Delta y = 500$ m horizontal resolution Cartesian grids (with $N_\sigma = 5$ vertical σ-layers) used to simulate SMFs sited in Areas 1-4 (numbered ellipses; Table 1); and (b) FUNWAVE: $\Delta x = \Delta y = 500$ m Cartesian resolution grid G0 encompassing the SMFs and their grids, and seven $\Delta x = \Delta y = 120$ m resolution Cartesian nested grids, labelled OC, AC, NJ, NY, MO, RI and NA (from southwest to northeast; Table 2).

7

Grids and SMFs	Area 1	Area 2	Area 3	Area 4
SW corner (Lon., Lat.)	(-75.00, 36.90)	(-74.32, 37.47)	(-75.97, 36.12)	(-76.37, 35.80)
center (x_0, y_0)	(-72.19, 39.19)	(-71.49, 39.76)	(-73.19, 38.41)	(-73.6, 38.09)
Azimuth θ (CW from N)	136°	153°	140°	126°

Table 1: Parameters of NHWAVE grids ($\Delta x = \Delta y = 500$ m resolution; $N_\sigma = 5$ σ-layers; 1,000 by 1,000 cells), and locations (center) of SMFs of width $b = 30$ km, width $w = 20$ km and thickness $T = 0.75$ km, in Areas 1-4 (Figs. 1 and 2a). For rigid slumps, the average local slope is assumed to be $\alpha = 4$ deg. (Fig. 3).

Grid Name	Cells (M_x, N_y)	Resol. (m)	SW Corner (Lat., Lon.)
Base Grid (G0)	(1600, 1600)	500	(34.82N, 76.37W)
Ocean City (OC)	(672, 1104)	120	(37.68N, 75.60W)
Atlantic City (AC)	(752, 1104)	120	(38.70N, 75.04W)
New Jersey (NJ)	(720, 936)	120	(39.70N, 74.40W)
New York (NY)	(1212, 792)	120	(40.49N, 74.21W)
Montauk (MO)	(780, 744)	120	(40.60N, 72.60W)
Rhode Island (RI)	(816, 828)	120	(40.90N, 71.65W)
Nantucket (NA)	(828, 832)	120	(40.81N, 70.67W)

Table 2: Parameters of FUNWAVE-TVD computational grids (Fig. 2)

m) resolution Northeast Atlantic and Southeast Atlantic U.S. Coastal Relief Models (NGDC, 1999a,b), wherever available (mostly up to the shelf break), and otherwise from the 1-arc minute resolution ETOPO-1 Global Relief Model (Amante and Eakins, 2009). The latter bathymetric data is plotted in Fig. 1, as both a color scale and contour lines, showing the typical pattern of the wide shallow USEC shelf (depth $h \leq 100m$) north of North Carolina, a steep shelf break slope and a deep abyssal plain ($h = 2,000$ to $5,000$ m). Similar to the Currituck slide complex, the four study areas 1-4 are all located on the shelf break slope.

3   SMF tsunami generation with NHWAVE(D)

3.1   SMF geometry, rheology and kinematics

As discussed above, we model tsunami generation by Currituck SMF proxies sited in Areas 1-4 off of the USEC (Fig. 1), assumed to fail as rigid slumps (similar to Grilli et al. (2015)) or as deforming slides (similar to that considered in Area 1 by Grilli et al. (2017b)). As in earlier work (Grilli et al., 2015), the Currituck SMF proxies all have an initial elliptical footprint of downslope length $b = 30$ km, width $w = 20$ km, and thickness $T = 0.75$, with a quasi-Gaussian geometry (Enet and Grilli, 2007; Grilli et al., 2015, 2017b); using a shape coefficient $\epsilon = 0.717$, this lyields a SMF volume $V_s = 158$ km^3 (see details in Appendix A). In NHWAVE(D), the initial SMF geometry
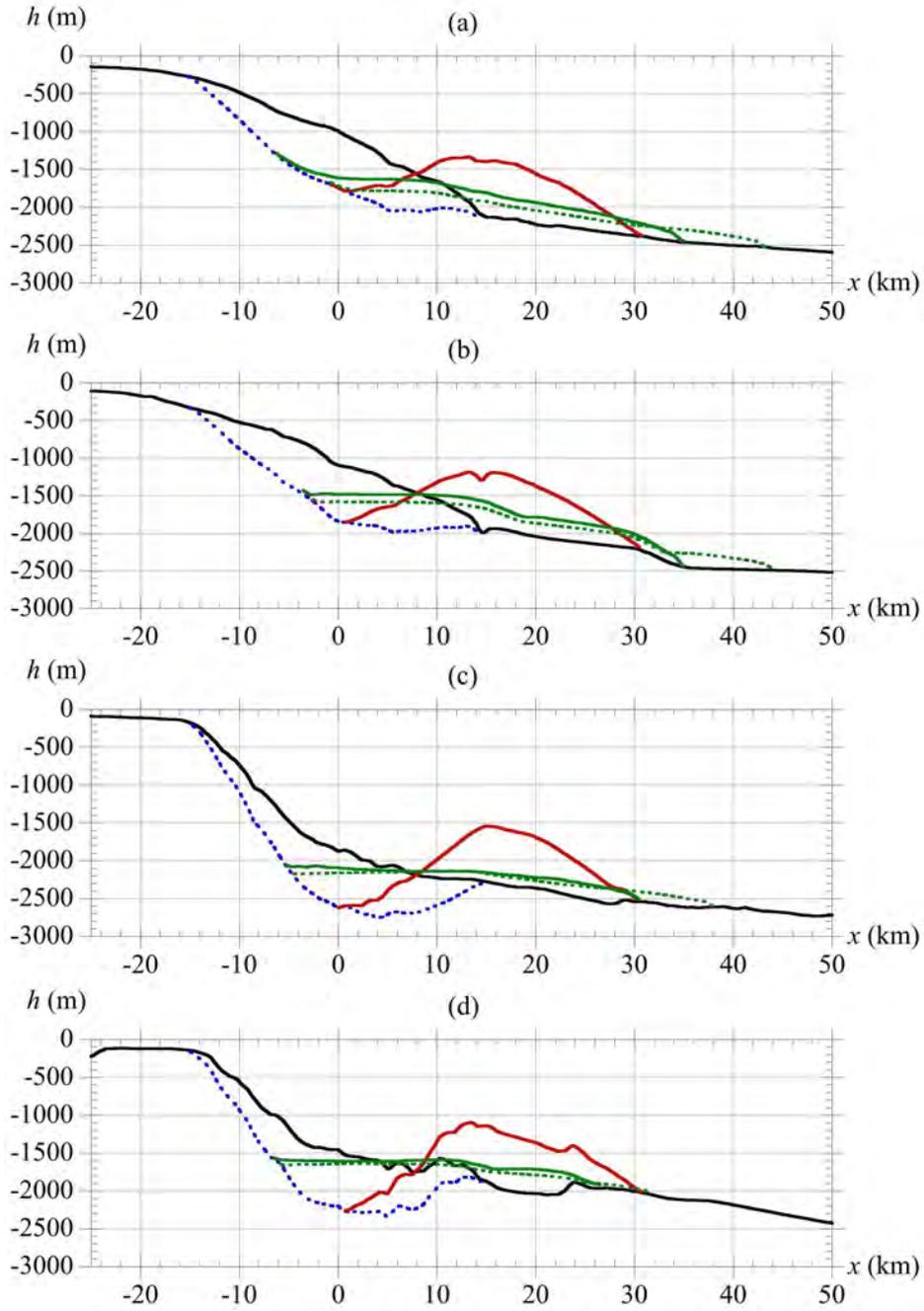
Figure 3: Vertical bathymetric transects in each NHWAVE grid (Fig. 2a), through Areas 1-4 (plots a-d) SMF centers (x_0, y_0), in azimuthal direction θ (Table 1): (solid black) current bathymetry; (dash blue) initial SMF profile; (solid red) final slump profile after displacement (runout) $S_f = 15.8$ km at $t_f = 715$ s (11.9 min); (solid green/dash green) deforming slide profiles at $t = 715$ and 1,200 s (20 min). The x-axis measures distances from each SMF center; vertical exaggeration is 25 times.

is specified below current seafloor (Fig. 3), with the elliptical footprint centered at longitude-latitude (x_0, y_0) and its major axis oriented downslope, in an initial azimuthal direction of motion θ (Table 1). Figure 3 shows vertical cross-sections in direction θ through the SMFs sited in Areas 1-4 (both seafloor bathymetry and initial/later SMF profiles). The SMFs are all sited on the continental shelf break slope, with the depth of their initial center of mass location varying between $d = 1,000$ and 1,800 m. The initial elliptical footprints of each SMF, with their orientation, are plotted in Fig. 6.

As in earlier work (Grilli and Watts, 2005; Grilli et al., 2015, 2017b), for rigid slumps, the bottom boundary conditions are analytically specified as a function of SMF geometry and other parameters, assuming a pendulum-like motion parallel to slope, $S(t)$ (see Eq. (4) in Appendix A). In this motion, maximum runout S_f and motion duration t_f are computed as a function of slump parameters: beside geometry, these include bulk sediment density $\rho_s = 1,900$ kg/m^3, water density $\rho_w = 1,025$ kg/m^3, average local slope α, radius of (pendulum) motion R, and (hydrodynamic) added mass coefficient C_M. In the transects of Fig. 3, average slopes are 3.2, 3.0, 4.0 and 3.1 deg., in the bathymetry above Areas 1-4 SMFs, respectively; however, considering that there are steeper parts in each transect, $\alpha = 4$ deg. was used for each slump, which also yields identical maximum runout and time of motion in each case. As in Grilli et al. (2015, 2017b), we use $C_M = 1$ and estimate the radius as, $R \simeq b^2/(8T) = 150$ km. With these parameters and applying Eqs. (4) to (10) in Appendix A, we find $S_f = 15.8$ km and $t_f = 715$ s (11.9 min). Fig. 3 shows the final profile of each rigid slump in Areas 1-4, for $t \geq t_f$, after they have moved a distance S_f down the slope.

The motion of deforming slides is modeled with the two-layer model NHWAVED, which computes it together with the SMF deformation and tsunami generation, based on the same initial geometry and bulk sediment density as for slumps, and on a specified SMF rheology. As in Grilli et al. (2017b), we consider the slide layer to behave as a dense Newtonian fluid, with rheology defined by the kinematic viscosity $\nu_s = 0.5$ m^2/s and the slide-to-substrate Manning friction coefficient $n = 0.1$ s^2/m$^{2/3}$. [Note that Grilli et al. (2017b) used this ν_s value in simulations, but wrongly listed the dynamic viscosity in their paper as $\mu_s = 500$ kg/(m.s), while it should have been 950 kg/(m.s), based on the bulk density.] Grilli et al. (2017b) observed in glass bead experiments that model results were not very sensitive to slide viscosity. Hence, they simulated the Currituck SMF as a deforming slide using this fairly high viscosity, which is in the range of suggested values for debris flows ($\nu_s = 0.2$-0.6 m^2/s), but compared results obtained for various substrate friction coefficients, $n = 0.05$, 0.10, or 0.15 s^2/m$^{2/3}$. Then, to compare tsunami generation for the deforming Currituck SMF with that simulated by Grilli et al. (2015) assuming a rigid slump, they used $n = 0.1$, which led to approximately the same maximum runout of the slump and slide center of mass at time $t_f = 11.9$ min, and a similar velocity of their center of mass during the first 10 min of each SMF motion. Grilli et al. (2017b) then simulated tsunami generation for a Currituck SMF proxy modeled as a deforming slide, sited in Area 1 off of the Hudson River canyon, using $\nu_s = 0.5$ m^2/s and $n = 0.05$, 0.10, or 0.15, to show the sensitivity of coastal impact to slide rheology. In the simulations performed here for

Currituck SMF proxies sited in Areas 1-4, modeled as deforming slides, we also use $\nu_s = 0.5 \text{ m}^2/\text{s}$, together with $n = 0.1$, which should make the deforming slide kinematics consistent with that of rigid slumps. Fig. 4 shows the kinematics computed during the NHWAVED simulations of these deforming slides, i.e., their center of mass motion $S(t)$, velocity $U(t)$, and acceleration $A(t)$, compared to that specified for rigid slumps in NHWAVE (see Appendix A).

Fig. 3 shows vertical cross-sections through deforming slides computed in Areas 1-4, in direction θ, at $t_f = 715$ s, the time the rigid slumps stop moving, and at $t = 1,200$ s (20 min), when NHWAVE(D)'s solution is moved into FTVD as an initial condition. At $t = t_f$, while the deforming slides' center of mass locations appear to be similar to those of the slumps, unlike the rigid slumps which have preserved their geometry and thickness all the way to the end of their motion, the deforming slides have flowed both downslope and sideways, leading to a significant reduction in thickness. For $t > t_f$, the deforming slides continue flowing down the slope, some by a considerable distance. However, due to both their reduced thickness and the large depth, they are no longer significantly tsunamigenic. This different behavior during motion as a function of SMF rheology is further detailed in Fig. 5, which shows the instantaneous 3D geometry at $t = 5$, 10, and 15 min, of the Currituck SMF proxy modeled in Area 1 (Fig. 1) with NHWAVE(D), either as a deforming slide or a rigid slump. The SMFs both start from the same initial elliptical footprint and geometry below seafloor, on the West side of the Hudson canyon apron (visible on the figures), but as time increases the deforming slide continuously flows down the steepest slope, while the rigid slump undertakes its forced pendulum motion in direction θ. In the case considered here, it is apparent that in the deforming slide, sediment flow asymmetrically, more towards the West side, whereas the slump stays symmetrical with respect to its axis of motion. This will lead to different alongshore tsunami generation in each case (see below). Finally, as the slump stops moving at $t_f = 11.9$ min, there is not much additional motion between $t = 10$ and 15 min, in Figs. 5d and f.

The SMF kinematics displayed in Fig. 4 are consistent with these observations. The theoretical laws of motion of rigid slumps are plotted as a reference, and are identical for slumps sited in Areas 1-4, which are all similarly parameterized. The figure confirms that slumps reach their maximum runout and stop moving at $t_f = 715$ s; they reach a maximum velocity $U_{max} = 34.7$ m/s at mid-course, and their acceleration is initially maximum at $A_0 = 0.153 \text{ m/s}^2$ and, after decreasing to zero and below, reaches an identical negative value at the end of the rigid motion. By contrast, the deforming slides all have a different center of mass kinematics, which are calculated as a function of the SMF deformation simulated in the bottom, dense fluid, layer of NHWAVED and hence is site specific to each area. At short time, Fig. 4c shows that the deforming slides' acceleration is larger than that of rigid slumps, up to $t = 60$-100 s, depending on the considered area. Consistent with the parameterization of Grilli et al. (2017b), in Areas 1-2, whose seafloor has a fairly simple convex shelf slope (Figs. 3a,b), the deforming slides reach a maximum velocity and runout at t_f similar to those of the slumps (Figs. 4a,b). In Areas 3-4, however, whose shelf slope is concave, despite having
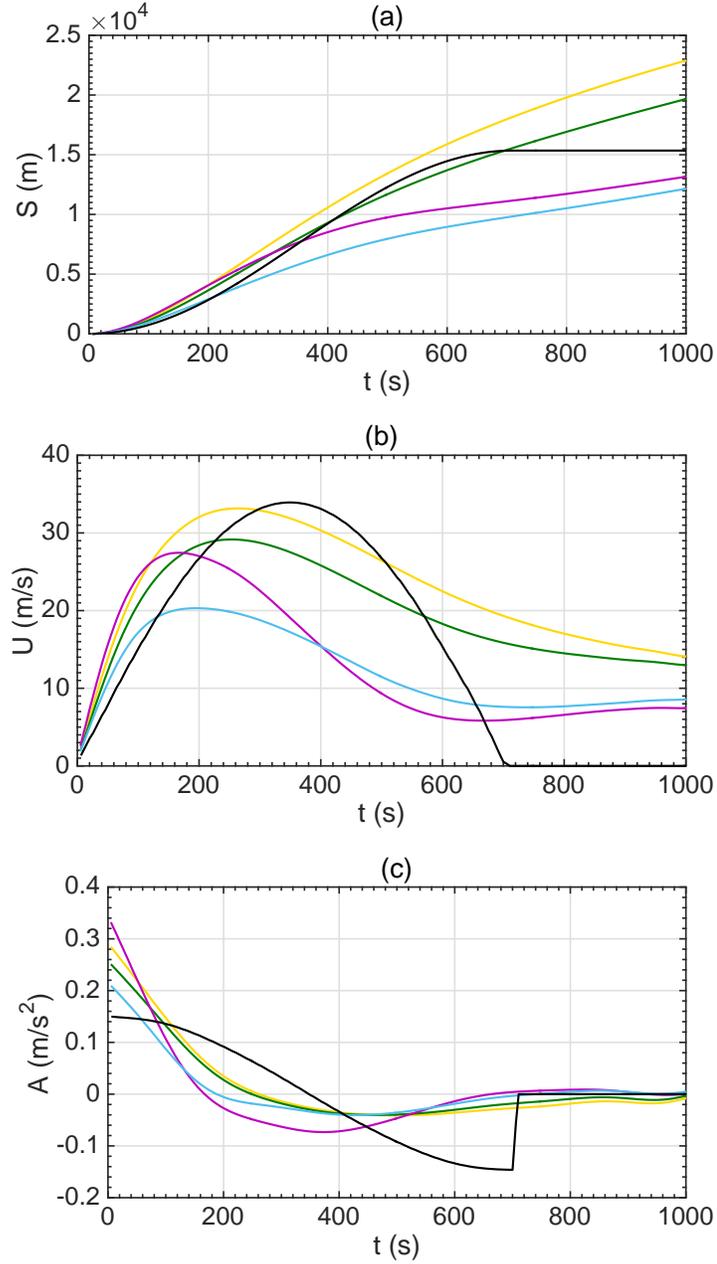
Figure 4: Kinematics of Currituck SMF proxies sited in Areas 1-4 (Fig. 1), during tsunami generation. SMF center of mass: (a) motion; (b) velocity; and (c) acceleration, specified for rigid slumps (black) modeled with NHWAVE (based on Eqs. (4) to (10) in Appendix A), and computed for deforming slides modeled with NHWAVED (for $\nu_s = 0.5$ m^2/s and $n = 0.1$), in Area: (ochre) 1; (green) 2; (purple) 3; (turquoise) 4.
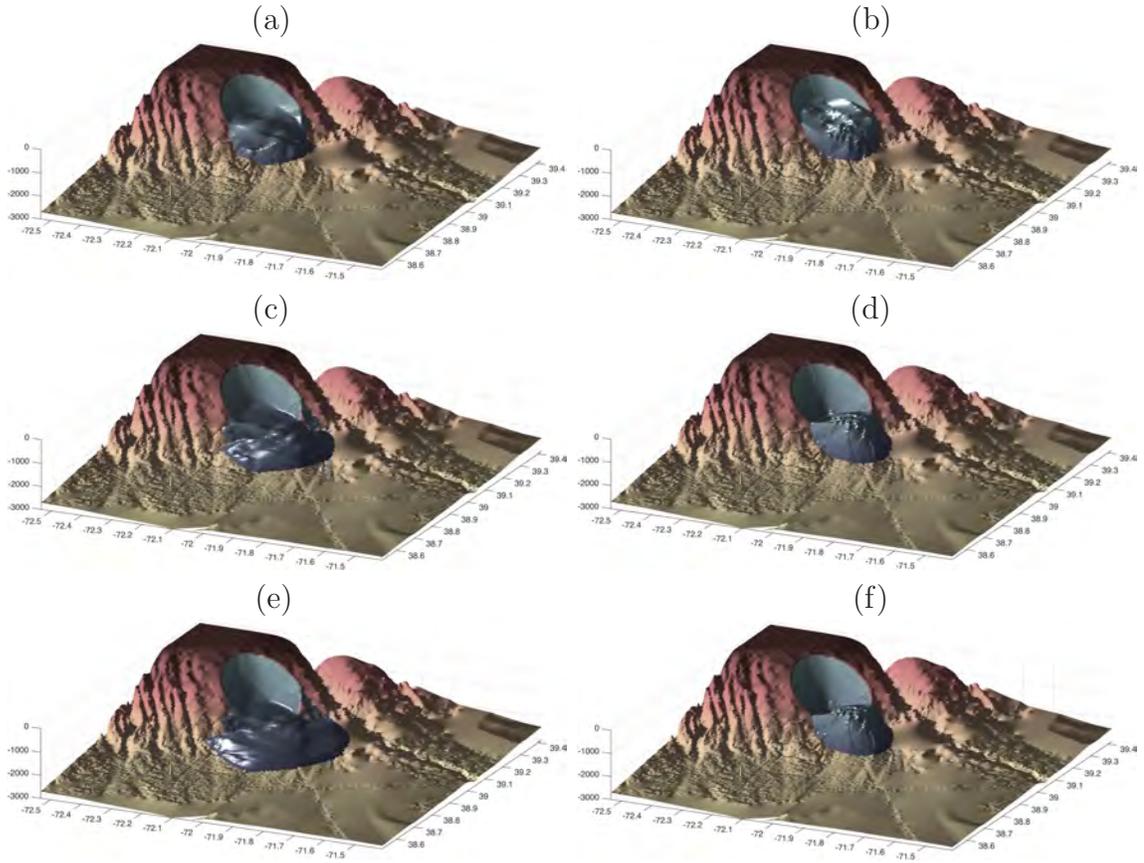
Figure 5: Instantaneous 3D geometry (grey volume) of Currituck SMF proxy in Area 1 (Fig. 1), simulated with NHWAVE(D) in a 500 m resolution grids with $N_\sigma = 5$ vertical layers (Fig. 2a), modeled as a: (a, c, e) deforming slide; or (b, d, f) rigid slump, at $t = $ (a, b) 5, (c, d) 10, and (e, f) 15 min. The vertical axis denotes depth in meter.

13

an initial motion similar to those of slides in the other two areas, up to $t \simeq 350$ s, the slides slow down quicker and reach a smaller runout at time t_f. This is clearly seen in transects of Figs. 3c,d, where in Areas 3-4, the slide material ends up filling the bottom of the initial cavity, which is below the deeper part of the shelf slope and hence only a smaller part of the slide continues a slower motion down the slope. This pattern of velocity and acceleration of deforming slides will lead to the generation of smaller onshore propagating, but larger offshore propagation tsunami waves compared to the rigid slumps.

3.2   Tsunami generation

Fig. 6 shows snapshots of surface elevations computed at $t = 800$ s (13.3 min), in simulations of tsunami generation for Currituck SMF proxies sited in Areas 1-4 (Fig. 1), performed using NHWAVE for rigid slumps (left panels) and NHWAVED for deforming slides (right panels). For each area, computations are made in individual grids with 500 m horizontal resolution and $N_\sigma = 5$ vertical layers (Fig. 2a; Table 1). As discussed before, the rigid slumps stop moving at $t_f = 715$ s, after covering a downslope runout distance $S_f = 15.8$ km (Fig. 3), at which time, by design, the deforming slides approximately have the same runout (see KINEMATICS FIG). While the rigid slumps keep their shape during motion, as discussed above, the deforming slides spread out and their thickness reduces during their downslope motion (Figs. 3 and NEW 3D FIG).

As expected from their similar kinematics (detailed above), Fig. 6 shows that, at $t = 800$ s, tsunami waves generated by rigid slumps and deforming slides have a similar overall pattern and horizontal spread (Fig. 6), but different elevations. In all cases, the onshore propagating tsunamis have a leading depression wave of 10-15 m elevation or more, followed by an equally large elevation wave; this leading wave, however, is larger for the rigid slumps. Additionally, since the deforming slides follow the bathymetry, they generate more asymmetric waves (alongshore) than the rigid slumps. At $t = 800$, in all cases, the offshore propagating tsunamis have a concentric (cylindrical) pattern, with a 5-10 m leading crest, followed by a deeper trough. Here, due to the slightly larger initial acceleration of the deforming slides (FIG) that has generated it, the leading crest elevation is larger for deforming slides than for rigid slumps.

Although the rigid slumps stop and no longer generate waves at $t_f = 715$ s, simulations are performed with NHWAVE(D) in both cases up to $t = 1,200$ s (20 min), before continuing simulations in FTVD, to make sure 3D effects have become negligible in the generated wave trains. At this time, Fig. 3 shows that the deforming slide profiles have large length-to-thickness ratios, and have reached a depth greater than 1500 m; hence they are no longer significantly tsunamigenic. Although the deforming slides have become very thin and thus only cause a small vertical velocity on the seafloor, as indicated before, to prevent triggering numerical instabilities in FTVD due to a mismatch in bottom boundary condition, flow velocities are filtered out of NHWAVE results, above the slide location, before initializing simulations in FTVD.

14
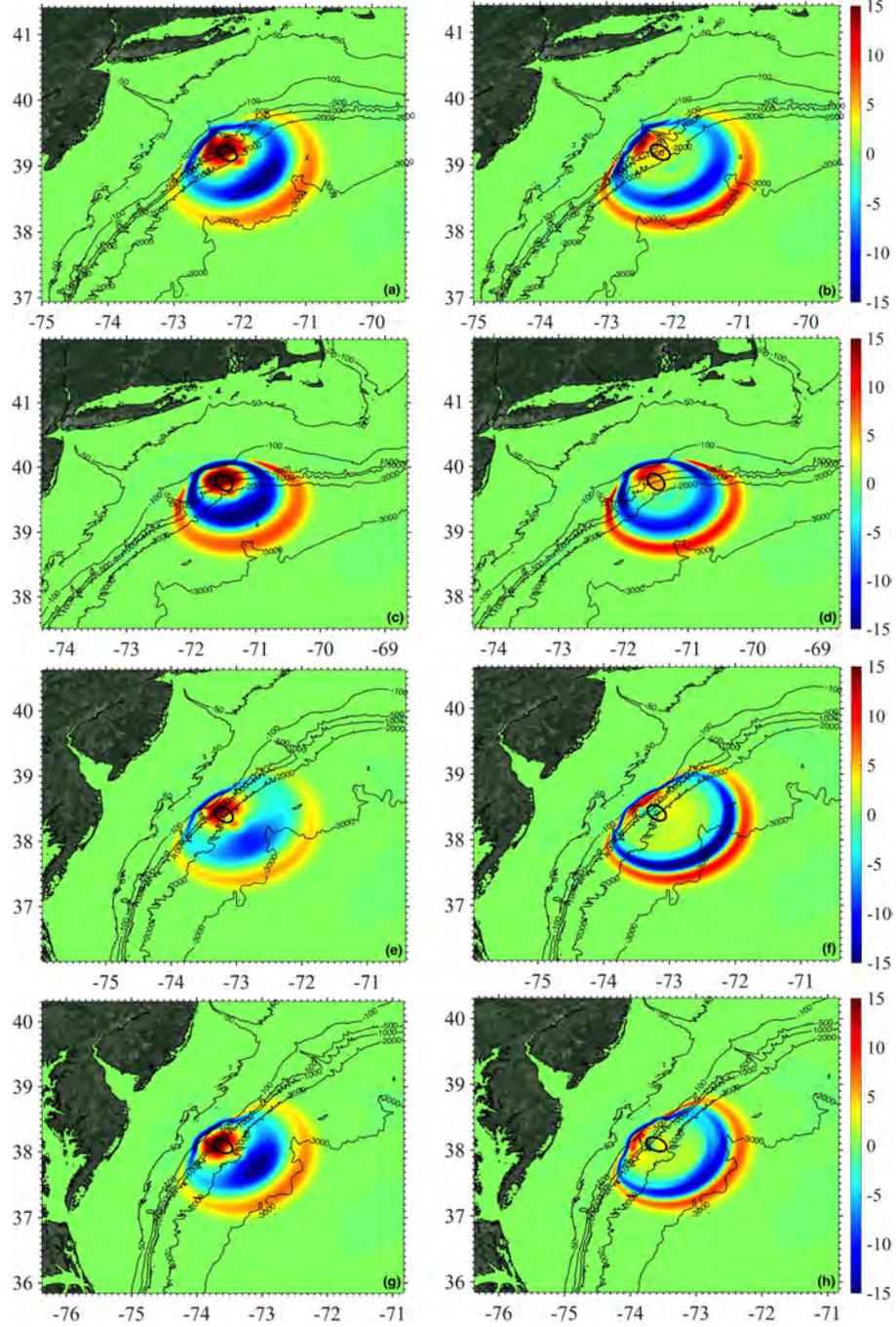
Figure 6: Snapshots of free surface elevations (color scale in m) simulated at $t = 800$ s (13.3 min) with NHWAVE(D), in 500 m grids (Fig. 2a; Table 1), for four Currituck SMF proxies modeled as: (a, c, e, g) rigid slumps (similar to Grilli et al., 2015); or (b, d, f, h) deforming slides (with $\nu_s = 0.5$ m/s^2, $n = 0.1$), sited in Areas 1-4 (Fig. 1). Black ellipses mark initial footprints of each SMF (Table 1), which all have a volume $V_s = 158$ km^3, density $\rho_s = 1900$ kg/m^3, and similar runout S_f at $t_f = 715$ s (when the slumps stop moving).

15
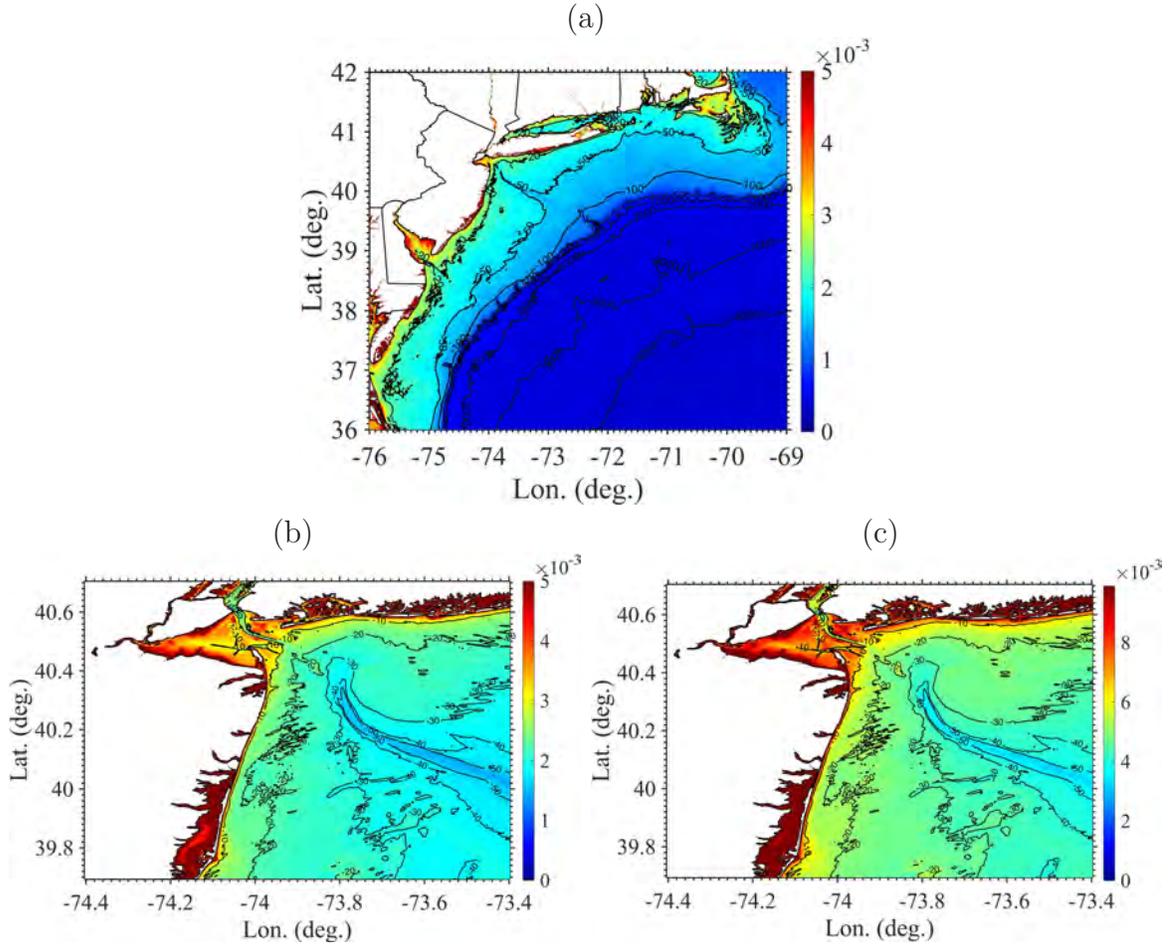
Figure 7: Spatial variation of friction coefficient $C_d = g\,n^2/h^{1/3}$ (color scale) used in FTVD simulations, based on local depth h (contour lines in meter) and Manning coefficient $n =$ (a) 0.025 over grid G0 (Fig. 2); (b, c) 0.025 and 0.0375 $\mathrm{s^2/m^{2/3}}$), respectively, over grid NJ (Fig. 2b; Table 2). Note, a minimum depth of 0.1 m is assumed in the C_d calculations.

16

4 Onshore tsunami propagation and coastal impact

The onshore propagation of tsunamis generated by rigid slumps and deforming slides sited in Areas 1-4 is simulated using FTVD. For each SMF, simulations are first performed in the 500 m resolution grid G0, initialized at $t = 20$ min with NHWAVE(D)'s results. Simulations are then continued by one-way coupling in the 7 nested, 120 m resolution, nearshore Cartesian grids (Fig. 2b; Table 2). In the simulations of tsunami generation with NHWAVE(D), which take place over short times in fairly large depth, bottom friction effects were neglected, except along the slide-to-substrate interface in NHWAVED, over which friction was modeled with a Manning $n = 0.1$. During the onshore tsunami propagation over the shallow continental shelf, however, bottom friction effects can significantly reduce tsunami elevations (Tehranirad et al., 2015; Grilli et al., 2015). Indeed, according to linear long wave theory, the tsunami depth-averaged current velocity U is proportional to $h^{-3/4}$ and, in FTVD, dissipation due to bottom friction is quadratic in U (Shi et al., 2012), i.e., $\propto C_d U^2$, with C_d the bottom friction coefficient. If C_d is modeled with Manning's formula as, $C_d = g\, n^2/h^{1/3}$, dissipation is, $\propto h^{11/6}$ and hence becomes significant over the shallow shelf. Accordingly, in FTVD simulations, bottom friction was specified based on Manning's formula. A value $n = 0.025$ s^2/m$^{2/3}$ was used throughout, but to assess the sensitivity of coastal inundation to bottom friction, simulations of the deforming slide sited in Area 1 were repeated using a larger value $n = 0.0375$ s^2/m$^{2/3}$, in grids G0 and NJ (Table 2); the latter grid encompasses the highly impacted areas of northern new Jersey and western Long island (Fig. 2b). Figure 7 shows maps of C_d values computed over grids G0 for $n = 0.025$ and G0 and NJ for $n = 0.0375$ (a minimum depth of 0.1 m was used in the model with respect to C_d calculations). In the first case (Figs. 7a,b), while C_d values are low in deeper water (less than 0.0015), they increase over the shelf to more than 0.002, and reach 0.003-0.005 values in less than 10 m depth; in the second case, C_d values are 2.25 times larger (Fig. 7c).

4.1 Instantaneous propagation and time series

Figure 8 shows a sequence of instantaneous surface elevations computed for a Currituck SMF proxy sited in Area 1, assuming a deforming slide, for $t = 10$ to 150 min by steps of 20 min. Tsunami generation is modeled with NHWAVED (upper left panel) and tsunami propagation is then modeled with FTVD in grid G0 (other panels). As time increases, while the initially onshore propagating tsunami waves continue their propagation towards the nearest shores, the northern and southern parts of the outgoing waves gradually refract over the shelf break bathymetry and eventually orient themselves parallel to the local isobaths, to propagate onshore towards the upper and lower parts of the coastline. Although there is some decrease in elevation down and up the coast due to energy spreading, the onshore propagating waves stay very large (several meters) over the entire study area. At 110 min (1h50'), Fig. 8 shows a nearly continuous elevation or depression wave, from south to north, propagating towards the
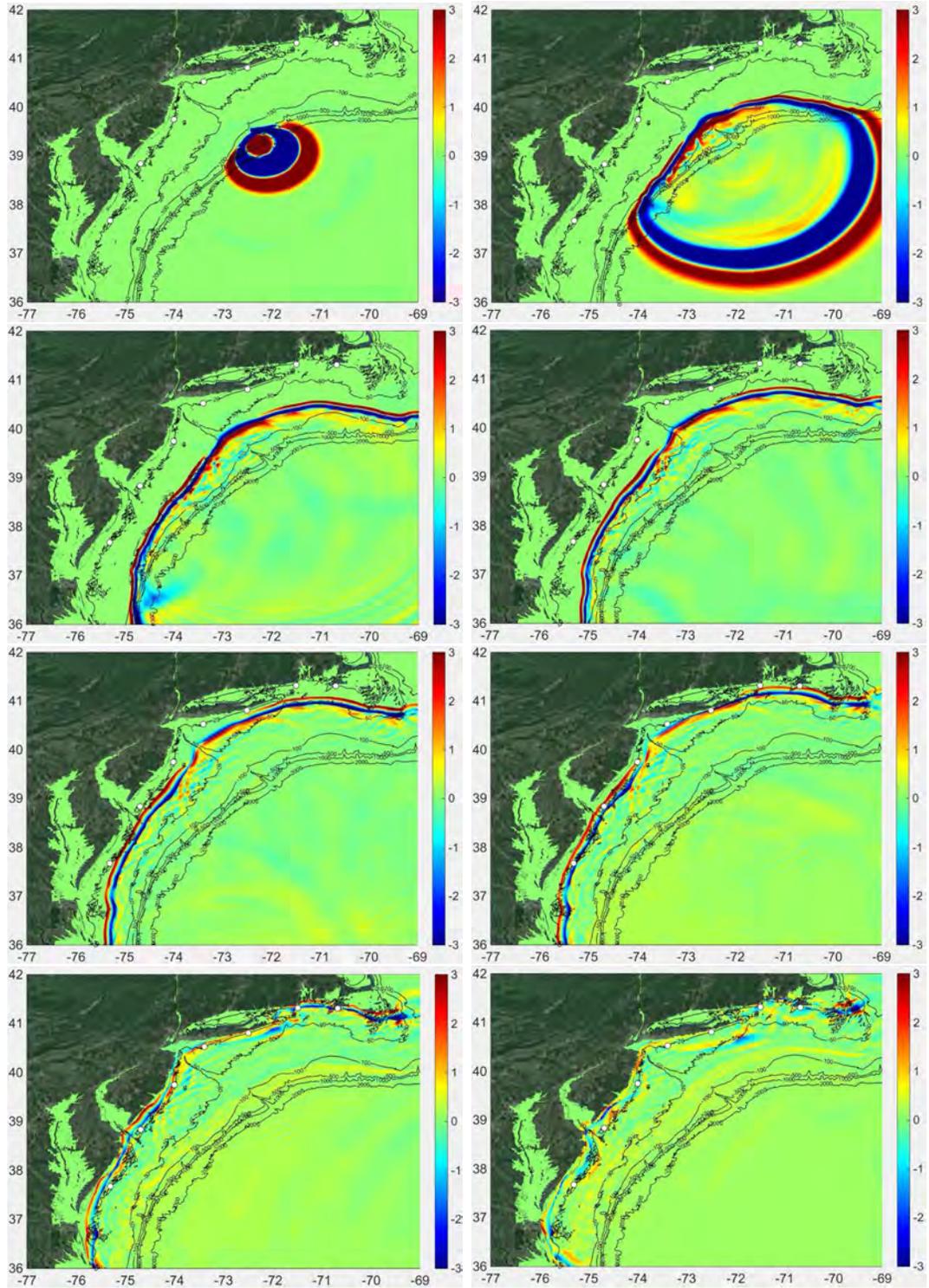
**Figure 8:** Instantaneous free surface elevations (color scale in m) simulated with NHWAVE and FTVD in grid G0 (Fig. 2) for the deforming Currituck SMF proxy in Area 1 (Figs. 1 and 6b) at $t = 10, 30, 50, 70, 90, 110, 130$, and 150 min (from left to right, up to down). Circles mark locations of gage stations 1-7 (Fig. 1). Black contours mark depth in meter.

18
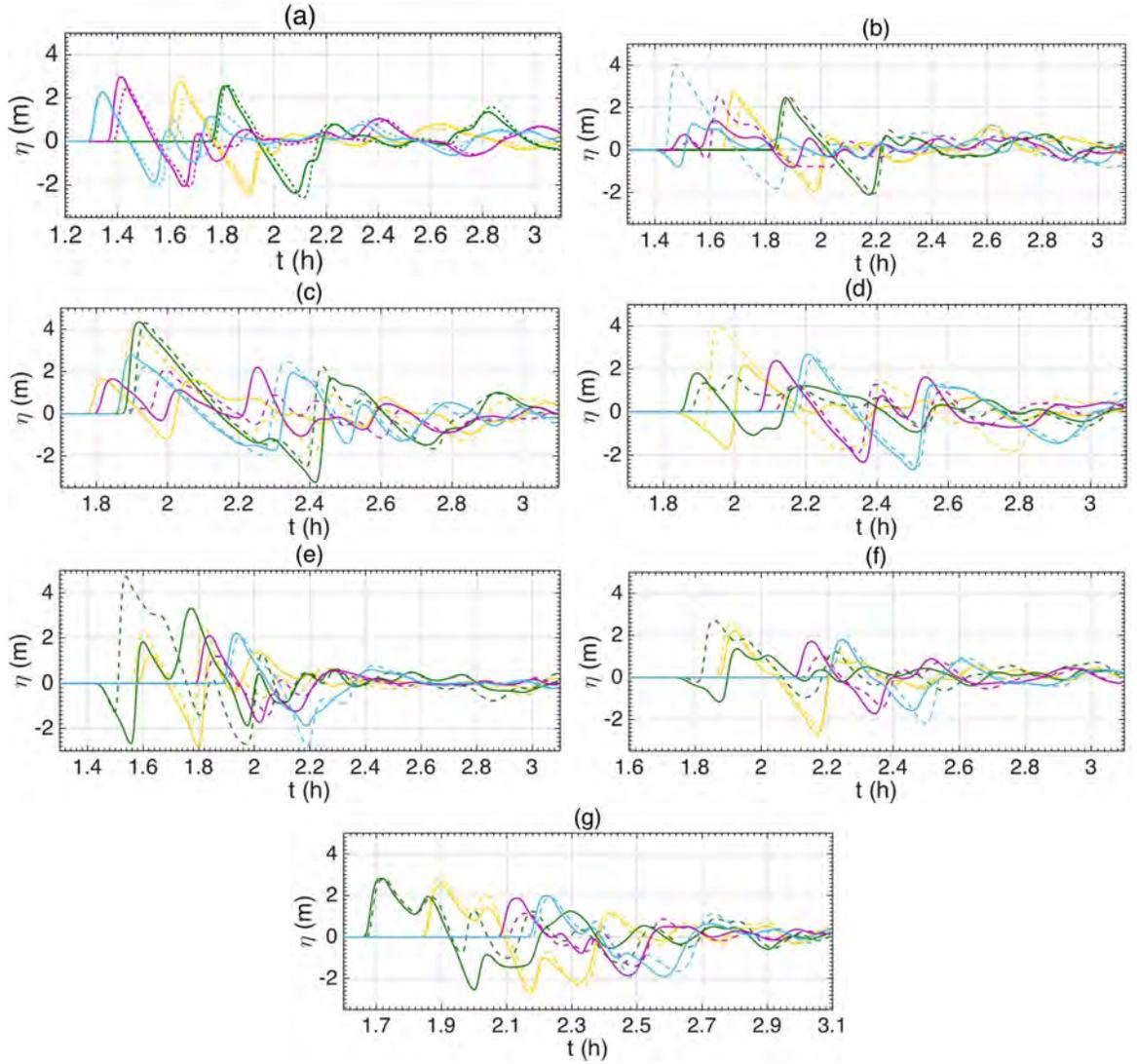
Figure 9: Time series of free surface elevation simulated with NHWAVE and FTVD in grid G0 (Fig. 2) at: (a-g) wave gage stations 1-7, as: (solid lines) rigid slumps; or (dash lines) deforming, Currituck SMF proxies, sited in Areas (Fig. 1): (ochre) 1; (green) 2; (purple) 3; and (turquoise) 4. All stations are located in 20 m depth and are at (Lon., Lat.): (1) (-75.30289, 37.67788); (2) (-74.68185, 38.83211); (3) (-73.99977, 39.74429); (4) (-73.39142, 40.52213); (5) (-72.48927, 40.80720); (6) (-71.49228, 41.31645); (7) (-70.67353, 41.31252).

coast, that approximately reaches the 20 m isobath at the same time (marked by the 7 white bullets denoting wave gage stations 1-7; Fig. 1). This means that the SMF tsunami generated in the Hudson river canyon in Area 1, ends up affecting the coast in the entire study area. This observation also applies to tsunamis generated by SMFs sited in other Areas 2-4.

When performing these simulations with FTVD for an increasing time in grid G0, it was observed for this and other SMF cases, that the outbound waves were not fully absorbed by the 125 km wide sponge layers specified along the eastern and southern boundaries of grid G0, which caused some reflection. Facing the same problem, Grilli et al. (2017b) filtered out the surface elevation and horizontal velocities of the outbound waves, before continuing simulations in one finer resolution nested grid; this however, affected the ability of outbound waves to refract up and down the coast. Here, to avoid resorting to such an arbitrary filtering and affecting tsunami impact up and down the coast, the footprint of grid G0 was extended by 400 km in both the east and south directions and simulations of each tsunami were pursued to $t = 50$ min (stage of 3rd panel in Fig. 8), at which time the outbound waves had propagated beyond the original offshore boundary of grid G0. Outbound waves were then simply truncated and simulations pursued in the original G0 grid up to $t = 186$ min (3h6'). During these simulations, in preparation for the one-way coupling to the 7 finer resolution nested grids (Fig. 2b), surface elevation and horizontal velocities were computed and saved every 5 s at the locations of all the boundary nodes of the finer nested grids.

Figure 9 shows time series of surface elevations computed with FTVD at wave gage Stations 1-7 (Fig. 1) in grid G0, for tsunamis generated by the 8 different Currituck SMF proxies sited in Areas 1-4 (both slumps and deforming slides). Note that all these stations are located in a 20 m depth on the boundary of one of the finer nested grids. Consistent with the instantaneous surface elevations shown in Fig. 8, depending on the SMF case and considered station, the incoming tsunami waves appear as either a depression or an elevation wave; and most of these leading waves take the form of a "sawtooth" shaped wave. For instance, for the deforming slide in Area 1 (Fig. 8), the tsunami arrives at all stations, but station 4, which is the most directly onshore of the source, as an elevation wave. Depending on the station and SMF considered, the period of the leading wave varies between 6 and 29 min, i.e., from quite short to much longer, and these waves are followed by a train of multiple waves, which can be shorter, or longer with many shorter waves riding on top of them. It should be pointed out that these simulations were performed in a fairly coarse 500 m resolution grid (G0), and it has been shown in earlier work, both experimental and numerical, that given a sufficiently fine spatial resolution, such long sawtooth-shaped waves, when properly measured or simulated in a dispersive wave model (such as FTVD), develop dispersive undular bores of shorter oscillations at both their crests and behind their troughs (Matsuyama et al., 2007; Madsen et al., 2008; Grilli et al., 2012, 2015).

20
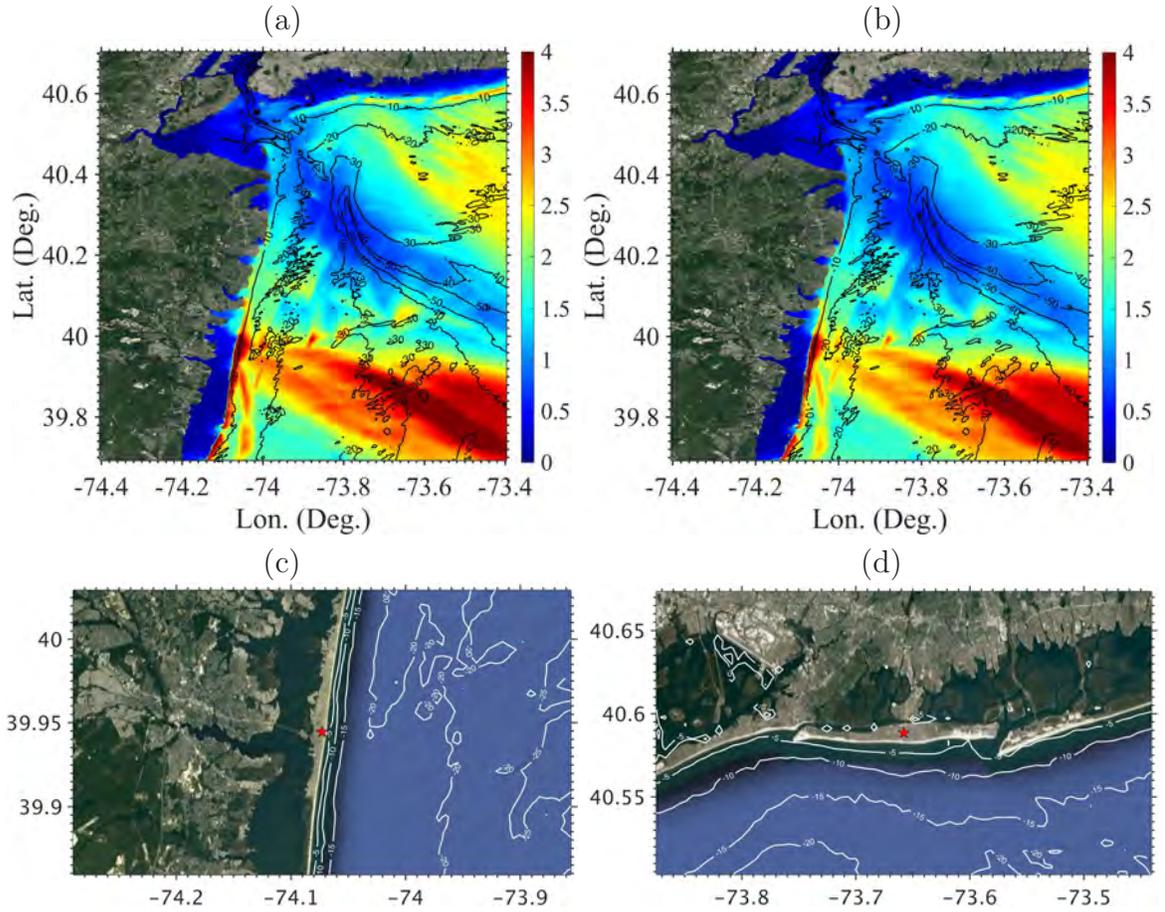
Figure 10: (a,b) Envelopes of maximum surface elevations (color scale in m) computed with FTVD in 120 m grid NJ (Fig. 2; Table 2), for the deforming Currituck SMF proxy sited in Area 1 (Figs. 1, 6b, and 8), with a Manning $n =$ (a) 0.025; or (b) 0.0375 s^2/m$^{2/3}$ (Figs. 7b,c). Black contours mark depth in meter. (c,d) zoom-in on the coastline and barrier beaches around Seaside Heights, NJ (c) and Long Beach, NY (d), both marked by red stars. White contours mark depth in meter
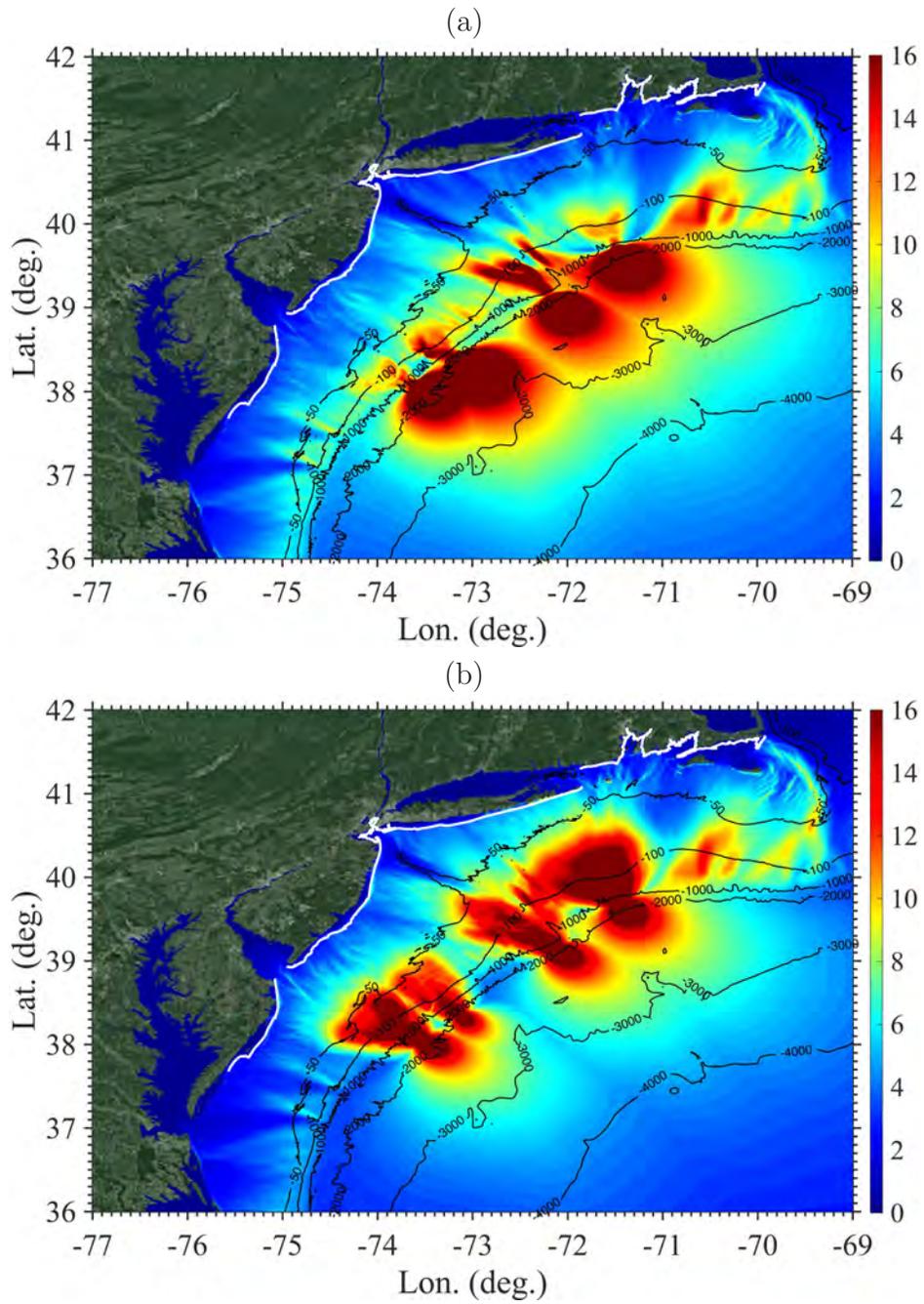
Figure 11: Combined envelope of maximum surface elevations (color scale in m) computed with FTVD in 500 m grid G0 or 120 m nested grids wherever available (Fig. 2b; Table 2), for the four SMFs sited in areas 1-4 (Fig. 1): (a) deforming slides; or (b) rigid slumps. The white lines mark the 5 m isobath along which maximum and minimum wave heights are computed (see, Fig. 12). Black contours mark depth in meter.
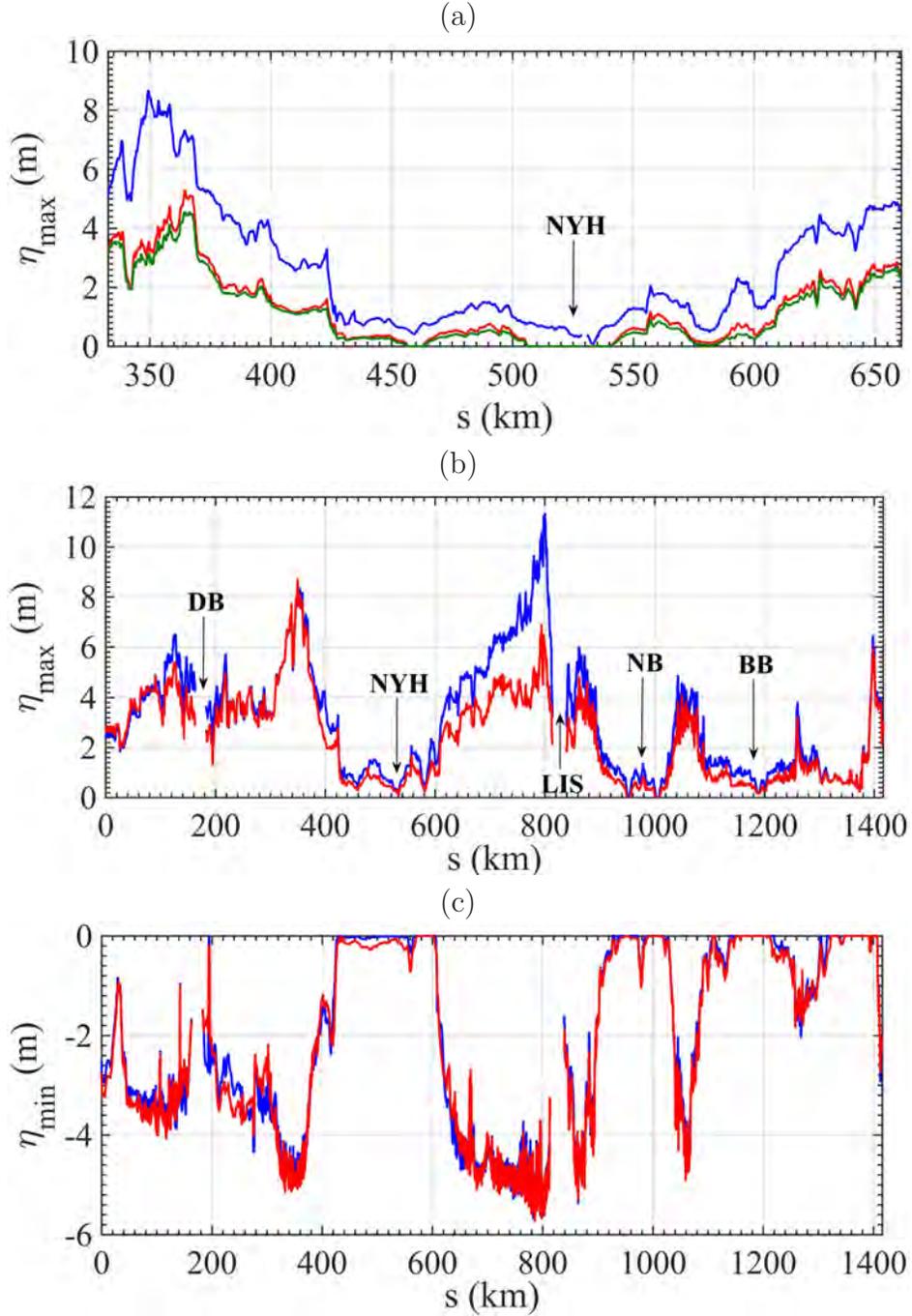
Figure 12: (a,b) Maximum and (c) minimum surface elevation computed along the 5 m isobath (Fig. 11) for tsunamis generated by: (blue) rigid slump in Area 1 (a), or combined slumps in Areas 1-4 (b,c); and (red) deforming slide in Area 1 (a), or combined deforming slides in Areas 1-4 (b,c). All FUNWAVE simulations are performed with $n = 0.025$ s^2/m$^{2/3}$; green line in plot (a) is deforming slide in Area 1 for $n = 0.0375$ s^2/m$^{2/3}$ (Fig. 7). The distance s is the curvilinear distance along the 5 m isobath measured from its southern end. Labels mark entrance to: (DB) Delaware Bay; (NYH) New York Harbor; (LIS) Long Island Sound; (NB) Narragansett Bay; (BB) Buzzards Bay.

23

4.2 Maximum and minimum surface elevations

Figure 10a shows the envelope of maximum surface elevation computed with FTVD in the 120 m resolution grid NJ (Fig. 2b; Table 2), for the deforming Currituck SMF proxy sited in Area 1 (Figs. 1), i.e., the same case as in Fig. 8. A Manning friction coefficient, $n = 0.025$ was used (Fig. 7b), as in grid G0,. As expected from earlier work (Grilli et al., 2015; Shelby et al., 2016) and seen in Fig. 8, due to the bathymetry of the Hudson River canyon, the incident tsunami, which is nearly parallel to the local isobath ahead of the canyon in 100 m depth (Fig. 8, second panel), gradually refracts away from the canyon and the entrance to New York Harbor, towards both northern New Jersey and western Long Island. Besides the snapshots of Fig. 8, this is clearly visible in the maximum surface elevations plotted in Fig. 10a, where there is a marked energy focusing towards the highly developed barrier beach of Seaside Height, NJ (Fig. 10c) and that of Long Beach, NY (Fig. 10d), over which maximum surface elevations of more than 4 and 2.5 m, respectively, are predicted, and the corresponding lagoons are fully flooded.

To assess the effect of bottom friction on tsunami coastal impact, the same simulation was repeated for a larger Manning friction coefficient, $n = 0.0375$ (Fig. 7c). Fig. 10b shows the envelope of maximum surface elevation computed with FTVD in 120 m resolution grid NJ. While the pattern of wave focusing-defocusing caused by refraction is not significantly affected, there is an overall reduction in maximum nearshore surface elevation, which is most clear along the barrier beaches skirting the coastline. This effect of friction on maximum tsunami inundation will be further illustrated and discussed below.

Fig. 11 shows the combined envelope of maximum surface elevations, separately computed for the 4 rigid slump and the 4 deforming Currituck SMF proxy cases. While offshore surface elevations significantly differ for the two different rheologies, particularly over the generation areas (in accordance with Fig. 6), patterns and directionality of maximum nearshore surface elevations are similar for the rigid slumps (Fig. 11a) and for the deforming slide (Fig. 11b) cases. This results from the strong bathymetric control on the focusing and defocusing of long tsunami waves, which start significantly refracting in fairly deep water (Tehranirad et al., 2015).

Figure 12 confirms this property of coastal tsunami impact, by plotting the maximum surface elevation, for the two rheologies, computed in the 120 m resolution grids, along the 5 m isobath (marked as a white line in Fig. 11 Chincoteague Island, VA, south of Ocean City, MD to Cape Cod, MA.), as a function of the curvilinear distance s measured along the isobath. In Fig. 12a, only results for the Currituck SMF proxy sited in Area 1, computed in grid NJ, are considered, for the rigid slump with $n = 0.025$ and deforming slide with either $n = 0.025$ (Fig. 10a) or $n = 0.0375$ (Fig. 10b). As observed before, the pattern of higher and lower maximum surface elevations is nearly identical for the 3 cases. As already noted by Grilli et al. (2017b), however, the maximum elevation of the deforming slide case is nearly half that of the rigid slump, and there is another small reduction in elevation when considering the larger friction, in

24

the latter case. Figure 12b plots the same results at the 5 m isobath, but combined for all 4 Currituck SMF proxies sited in Areas 1-4, simulated in the 7 nested grids, and for both rheologies (as in Fig. 11). Here the picture seems more complex, as we have seen that all SMF sources can generate tsunamis that affect the entire upper USEC in some manner, due to wave refraction over the complex geometry of the shelf break. While the rigid slumps still cause the maximum inundation, with 11.5 m around the eastern end of long Island near Montauk, NY ($s = 800$ km; Fig. 1), where the shelf bathymetry is particularly concave and causes high wave focusing, the reduction in coastal impact when considering deforming slides is overall less marked. For deforming slides, the maximum inundation is reduced to 8.5 m and now occurs near Atlantic City, NJ ($s = 350$ km; Fig. 1), while in Montauk the impact is reduced to 7 m. In these combined envelopes, the pattern of wave focusing and defocusing repeats itself, with the lowest impact occurring in or near Bays and estuaries (e.g., Delaware Bay, New York harbor, Narragansett Bay, Buzzards Bay).

Finally, Fig. 12c shows the envelope of minimum surface elevations simulated at the 5 m isobath, for the combination of the 4 Currituck SMF proxies sited in Areas 1-4, simulated in the 7 nested grids, and for both rheologies. Such results would be important for instance when considering tsunami impact effects on the fresh water intakes of a power plant, of which there are a few in this area (e.g., nuclear power plants in Millstone, CT near the mouth of Long Island Sound or Oyster Creek, NJ, just south of Seaside Height). Here, results appear quite similar for the rigid slump and deforming slide cases; at a few instances, in particular near Atlantic City ($s = 350$ km) and Montauk ($s = 800$ km), the minimum elevation would reach down to the seafloor (i.e., 5 m; with some minor irregularities related to discretization and the moving shoreline algorithm). This similarity in minimum values is expected since the minimum coastal elevation is typically caused by the depression wave that first arrives on the nearest shores facing Areas 1-4 (Figs. 1 and 9), and it is a result of the initial motion of each SMF, i.e., at short time when deformation has not yet played an important role, but instead SMF mass, initial acceleration, and local slope control wave generation (Grilli and Watts, 2005).

5   Discussion and conclusions

In their probabilistic analysis (MCS) of landslide tsunami hazard along the USEC, Grilli et al. (2009) concluded that the 500 year tsunami runup along the upper USEC was largest from Virginia to Cape Cod (about 6-7 m maximum). Additional MCS and geotechnical analyses identified 4 areas (Fig. 1) where large SMFs were both possible due to large sediment accumulation and most probable due to low factor of safety in slope stability analyses (Krauss, 2011; Eggeling, 2012). In light of this, with the aim to simulate Probable Maximum Tsunamis (PMTs), Grilli et al. (2015) performed direct simulations for extreme SMFs having the lumped characteristics of the historical Currituck slide complex (i.e., "Currituck SMF proxies"; 30 km long by

20 m wide by 0.75 km maximum thickness), and to maximize coastal impact modeled them as rigid slumps. The coastal inundation caused by these SMF tsunamis was combined with that caused by other PMTs from extreme sources identified in the Atlantic Ocean (Grilli et al., 2010; Tehranirad et al., 2015; Grilli et al., 2017a), to produce the first generation of tsunami inundation maps for the most exposed areas of the USEC to tsunami hazard, under the auspice of the National Tsunami Hazard Mitigation Program (NTHMP) (Tehranirad et al., 2014, 2015a,b,c,d,e). The present study was performed in the context of this earlier work, as newer model simulating different slide rheologies became available (Kirby et al., 2016; Grilli et al., 2017b), and considering that all SMFs failed as rigid slump was being questioned as being perhaps too conservative.

Thus, in this work, while still considering Currituck SMF proxies sited in Areas 1-4 (with a 158 km^3 volume), we performed new numerical simulations to assess how tsunami hazard along the upper US East Coast is affected by SMF rheology, i.e., whether the SMFs behave as rigid slumps or deforming slides. Based on earlier work (Grilli et al., 2017b), the latter were assumed to have the same bulk density as rigid slumps ($\rho_s = 1,900$ kg/m^3), a fairly large viscosity in the upper range of debris flows ($\nu_s = 0.5$ m/s^2), and a substrate to slide Manning friction coefficient $n = 0.1$. As these simulations used higher resolution grids than before, and to perform a detailed comparison, besides tsunami generation from deforming slides, we re-simulated tsunami generation for the rigid slumps considered by Grilli et al. (2015). In all cases, tsunami generation was simulated using the 3D non-hydrostatic model NHWAVE (for slumps) (Ma et al., 2012) and the two-layer NHWAVED model (for deforming slides) (Kirby et al., 2016), and the initial SMF geometry was assumed to be quasi-Gaussian (below current seafloor) with an elliptical footprint on the slope. For rigid slumps, both time varying geometry and law of motion were specified as bottom boundary conditions (Grilli and Watts, 2005; Watts et al., 2005; Grilli et al., 2015) and, for deforming slides, SMF motion and deformation were directly modeled in NHWAVED, as a depth-integrated bottom layer of dense Newtonian fluid, fully coupled to the overlying fluid motion modeled with the standard σ-layer NHWAVE. Once the SMFs were no-longer tsunamigenic (i.e., the slumps had stopped moving or the slides were deep and thin enough), we continued simulating tsunami propagation using the 2D fully nonlinear and dispersive long wave model FUNWAVE-TVD. For the onshore tsunami propagation, we use nested grids of 500 and 120 m resolution and applied our standard one-way coupling methodology.

Results of tsunami generation simulations showed that deforming slides, while having a slightly larger initial acceleration, generated smaller onshore propagating tsunamis than rigid slumps, due to their spreading and thinning out during motion, which gradually makes them less tsunamigenic; by contrast, rigid slumps kept their specified shape during their pendulum-like motion. Also, since they flowed down the slope following the terrain, deforming slides caused more asymmetric tsunamis along-shore, with respect to their initial direction of motion, than rigid slumps (Fig. 5). The offshore-propagating tsunami waves were usually as large or larger than for slumps (Fig.

26

6). Effects of SMF rheology on coastal tsunami impact, were evaluated by comparing the combined maximum envelope of surface elevation caused nearshore and along the shore over the 5 m isobath, by tsunamis generated by the 4 rigid slumps or deforming slides (Fig. 12). Consistent with earlier work (Tehranirad et al., 2015, 2017; Grilli et al., 2017b), we found that the bathymetry of the wide shelf has strong, first-order, control on the magnitude of tsunami coastal inundation, as it induces wave focusing and defocusing effects. Additionally, tsunami propagation and refraction over the shelf, both north and south of each source area, causes non-trivial variations in surface elevation and coastal inundation. This implies that a given SMF can generate tsunami waves that cause a significant coastal impact far alongshore from their source area. Overall, as expected from earlier work (Grilli and Watts, 2005; Grilli et al., 2017b), tsunamis caused by rigid slumps were found to be worst case scenarios, causing the largest maximum inundation at all sites (with a maximum of about 11.5 m around Montauk, NY), and up to 50% more inundation than for the slides considered here, which had a moderate level of deformation. For rigid slumps, the maximum computed inundation of 8-11.5 m at the 5 m isobath is larger than the estimated 500 runup of 6-7 m by Grilli et al. (2009), also based on rigid slumps (or slides) assumptions. This could be expected since the Currituck SMF proxies considered here were aimed at causing PMTs for the upper USEC, with potentially thousands of years return periods (the estimated age of the Currituck slide complex is about 16Ka). By contrast, the maximum inundation of 8.5 m computed here for deforming slides (around Atlantic City) is more consistent with the 500 year runup estimated in earlier work based on MCS. This could indicate that the return period of the largest events was underestimated in the MCS work. Regarding minimum elevations at the coast, which affect power plant intakes, tsunamis from both types of SMFs were shown to be able to cause water withdrawal to the 5 m isobath or deeper. Finally, the effects of bottom friction on tsunami coastal inundation were assessed by performing simulations for the Area 1 deforming slide in the 120 m NJ grid, using two different Manning coefficients, one 50% larger than the other. Using the increased friction from $n = 0.025$ to 0.375, led to a reduction of the largest tsunami inundations at the coast, in some cases, by up to 15%. Smaller inundation levels were less noticeably affected.

In conclusion, it seems that unless tsunami hazard assessment is performed for a critical coastal facility (such as a nuclear power plant), which requires considering the most extreme PMTs, it appears more realistic for standard tsunami hazard assessment (such as the NTHMP inundation mapping) to consider moderately deforming SMFs, whose center of mass follows a similar kinematics as that of the rigid slumps but whose deformation leads to reduce coastal impact. This is also consistent with paleo-SMF observations made on the upper East coast continental shelf and margin (ten Brink et al., 2014). Considering its marked effect on maximum inundation, values of the bottom friction coefficient should be carefully selected, particularly nearshore. Additional nearshore simulations of coastal inundation, in high-resolution grids (e.g., 30 m), caused by the deforming slide PMTs will be left out for future work.

Acknowledgments

References

Abadie S, Harris JC, Grilli ST and R Fabre (2012). Numerical modeling of tsunami waves generated by the flank collapse of the Cumbre Vieja Volcano (La Palma, Canary Islands) : tsunami source and near field effects. J Geophys Res, 117:C05030, doi:10.1029/2011JC007646.

Amante C and BW Eakins (2009). ETOPO1 1 Arc-Minute Global Relief Model: Procedures, Data Sources and Analysis. NOAA Technical Memorandum NESDIS NGDC-24. National Geophysical Data Center, NOAA. doi:10.7289/V5C8276M [March 15, 2017].

ECMAP 2017. NTHMP tsunami inundation maps for the US East Coast. https://www.udel.edu/kirby/nthmp.html.

Eggeling T (2012). Analysis of earthquake triggered submarine landslides at four locations along the U.S. east coast. Masters Thesis. University of Rhode Island.

Enet F, and ST Grilli (2007). Experimental Study of Tsunami Generation by Three-Dimensional Rigid Underwater Landslides. J. Waterway, Port, Coastal, Ocean Eng. 133(6):442-454. doi: 10.1061/(ASCE)0733-950X(2007)133:6(442).

Fine I.V., Rabinovich AB, Bornhold BD, Thomson R and EA Kulikov (2005) The Grand Banks landslide-generated tsunami of November 18, 1929: preliminary analysis and numerical modeling. Mar Geol, 215:45-57.

Geist E, P Lynett and J Chaytor (2009). Hydrodynamic modeling of tsunamis from the Currituck landslide. Marine Geology, 264:41-52, doi:10.1016/j.margeo.2008.09.005.

Glimsdal S, Pedersen GK, Harbitz CB and F Løvholt (2013). Dispersion of tsunamis: does it really matter ? Nat. Hazards Earth Syst. Sci., 13:1507-1526, doi:10.5194/nhess-13-1507-2013.

Grilli ST and P Watts (1999). Modeling of waves generated by a moving submerged body. Applications to underwater landslides. Engng Analys Boundary Elements, 23:645-656.

Grilli ST and P Watts (2005). Tsunami Generation by Submarine Mass Failure. I: Modeling, Experimental Validation, and Sensitivity Analyses. J. Waterway, Port, Coastal, Ocean Eng. 131(6):283-297. doi:10.1061/(ASCE)0733-950X(2005)131:6(283).

Grilli ST, Taylor O-DS, Baxter CDP and S Maretzki (2009). Probabilistic approach for determining submarine landslide tsunami hazard along the upper East Coast of the United States. Mar Geol 264(1-2):74-97.

Grilli ST, Dubosq S, Pophet N, Pérignon Y, Kirby JT and F Shi (2010). Numerical simulation and first-order hazard analysis of large co-seismic tsunamis generated in the Puerto Rico trench: near-field impact on the North shore of Puerto Rico and far-field impact on the US East Coast. Nat Haz Earth Syst Sc, 10:2109-2125, doi:10.5194/nhess-2109-2010.

GrilliJ ST, Harris JC, Tappin DR, Masterlark T, Kirby JT, Shi F and G Ma (2012). Numerical modeling of coastal tsunami dissipation and impact. In Proc. 33rd Intl. Coastal Engng. Conf. (P. Lynett and J. Mc Kee Smith, eds.) (ICCE12, Santander, Spain, July, 2012), 12 pps. World Scientific Publishing Co. Pte. Ltd.

Grilli ST, Harris JC, Tajalibakhsh T, Masterlark TL, Kyriakopoulos C, Kirby JT and F Shi (2013). Numerical simulation of the 2011 Tohoku tsunami based on a new transient FEM co-seismic source: Comparison to far- and near-field observations. Pure Appl. Geophys., 170:1333-1359, doi:10.1007/s00024-012-0528-y.

Grilli ST, O'Reilly C, Harris JC, Tajalli Bakhsh T, Tehranirad B, Banihashemi S, Kirby JT, Baxter CDP, Eggeling T, Ma G and F Shi (2015). Modeling of SMF tsunami hazard along the upper US East Coast: detailed impact around Ocean City, MD. Nat Hazards 76(2):705-746. doi:10.1007/s11069-014-1522-8.

Grilli ST, Grilli AR, Tehranirad B and JT Kirby (2017a). Modeling tsunami sources and their propagation in the Atlantic Ocean for coastal tsunami hazard assessment and inundation mapping along the US East Coast. In Proc. Coastal Structures and Solutions to Coastal Disasters 2015 : Tsunamis (Boston, USA. September 9-11, 2015), American Soc. Civil Eng., pps. 1-12.

Grilli ST, Shelby M, Kimmoun O, Dupont G, Nicolsky D, Ma G, Kirby JT and F Shi (2017b). Modeling coastal tsunami hazard from submarine mass failures: effect of slide rheology, experimental validation, and case studies off the US East Coast. Nat Hazards 86(1),353-391. doi:10.1007/s11069-016-2692-3.

Hill JC, Brothers DS, Craig BK, Uri S, Chaytor JD and CH Flores (2017). Geologic controls on submarine slope failure along the central US Atlantic margin:

Insights from the Currituck Slide Complex. Marine Geology, 385:114-130. doi: 10.1016/j.margeo.2016.10.007.

Kirby JT, Shi F, Tehranirad B, Harris JC and ST Grilli (2013). Dispersive tsunami waves in the ocean: Model equations and sensitivity to dispersion and Coriolis effects. Ocean Modell, 62:39-55, doi:10.1016/j.ocemod.2012.11.009.

Kirby JT, Shi F, Nicolsky D and S Misra (2016). The 27 April 1975 Kitimat, British Columbia submarine landslide tsunami: a comparison of modeling approaches. Landslides,13(6):1421-1434. doi: 10.1007/s10346-016-0682-x.

Krauss T (2011). Probabilistic tsunami hazard assessment for the United States East Coast. Masters Thesis. University of Rhode Island. http://chinacat.coastal.udel.edu/nthmp/krause-ms-uri11.pdf.

Locat J, Lee H, ten Brink US, Twitchell D, Geist E and M Sansoucy (2009). Geomorphology, stability and mobility of the Currituck slide. Mar Geol 264:28-40.

Løvholt F, Pedersen G and G Gisler (2008). Oceanic propagation of a potential tsunami from the La Palma Island. J Geophys Res, 113:C09026.

Ma G, Shi F and JT Kirby (2012). Shock-capturing non-hydrostatic model for fully dispersive surface wave processes. Ocean Modell, 43-44:22-35.

Madsen PA, Fuhrman DR and HA Schaffer (2008). On the solitary wave paradigm for tsunamis. J Geophys Res, 113, C12012, 22 pp.

Matsuyama M, Ikeno M, Sakakiyama T and T Takeda (2007). A study of tsunami wave fission in an undistorted experiment. Tsunami and Its Hazards in the Indian and Pacific Oceans. Pure Appl Geophys, 164:617-631.

National Geophysical Data Center (1999a). U.S. Coastal Relief Model - Northeast Atlantic. National Geophysical Data Center, NOAA. doi:10.7289/V5MS3QNZ [March 15, 2017].

National Geophysical Data Center (1999b). U.S. Coastal Relief Model - Southeast Atlantic. National Geophysical Data Center, NOAA. doi:10.7289/V53R0QR5 [March 15, 2017].

Piper DJW, Cochonat P and ML Morrison (1999). The sequence of events around the epicentre of the 1929 Grand Banks earthquake: initiation of the debris flows and turbidity current inferred from side scan sonar. Sedimentology, 46:79-97.

SLIDE (2017). Slope Stability Analysis Model. RockScience Inc. https://www.rocscience.com/rocscience/products/slide.

Shelby, M, Grilli ST and AR Grilli (2016). Tsunami hazard assessment in the Hudson River Estuary based on dynamic tsunami tide simulations. Pure Appl Geophys,173(12), 3,999-4,037, doi:10.1007/s00024-016-1315-y.

Shi F, Kirby JT, Harris JC, Geiman JD and ST Grilli (2012). A high-order adaptive time-stepping TVD solver for Boussinesq modeling of breaking waves and coastal inundation. Ocean Modell, 43-44:36-51, doi:10.1016/j.ocemod.2011.12.004.

Tappin DR, Watts P and ST Grilli (2008). The Papua New Guinea tsunami of 1998: anatomy of a catastrophic event. Natural Hazards and Earth System Sciences, 8:243-266.

Tappin DR, Grilli ST, Harris JC, Geller RJ, Masterlark T, Kirby JT, F Shi, G Ma, Thingbaijamg KKS and PM Maig (2014). Did a submarine landslide contribute to the 2011 Tohoku tsunami ? Marine Geology, 357:344-361 doi: 10.1016/j.margeo.2014.09.043.

Tehranirad B, Banihashemi S, Kirby JT, Callahan JA and F Shi (2014). Tsunami inundation mapping for Ocean City, MD NGDC DEM. Research Report No. CACR-14-04, Center for Applied Coastal Research, Department of Civil and Environmental Engineering, University of Delaware.

Tehranirad B, Harris JC, Grilli AR, Grilli ST, Abadie S, Kirby JT and F Shi (2015). Far-field tsunami hazard in the north Atlantic basin from large scale flank collapses of the Cumbre Vieja volcano, La Palma. Pure Appl Geophys, 172(12):3,589-3,616, doi:10.1007/s00024-015-1135-5.

Tehranirad B, Kirby JT, Callahan JA and F Shi (2015a). Tsunami inundation mapping for Atlantic City, NJ NGDC DEM. Research Report No. CACR-15-01, Center for Applied Coastal Research, Department of Civil and Environmental Engineering, University of Delaware.

Tehranirad B, Kirby JT, Callahan JA and F Shi (2015b). Tsunami inundation mapping for the northern half of the State of New Jersey. Research Report No. CACR-15-02, Center for Applied Coastal Research, Department of Civil and Environmental Engineering, University of Delaware.

Tehranirad B, Kirby JT, Callahan JA and F Shi (2015c). Tsunami inundation mapping for New York City. Research Report No. CACR-15-03, Center for Applied Coastal Research, Department of Civil and Environmental Engineering, University of Delaware.

Tehranirad B, Kirby JT, Callahan JA and F Shi (2015d). Tsunami inundation mapping for Montauk, NY NGDC DEM. Research Report No. CACR-15-04, Center for Applied Coastal Research, Department of Civil and Environmental Engineering, University of Delaware.

Tehranirad B, Kirby JT, Callahan JA and F Shi (2015e). Tsunami inundation mapping for Nantucket, MA NGDC DEM. Research Report No. CACR-15-05, Center for Applied Coastal Research, Department of Civil and Environmental Engineering, University of Delaware.

Tehranirad B, Kirby JT, Grilli ST, Grilli AR and F. SHi (2017). Continental Shelf Bathymetry Controls the Spatial Distribution of Tsunami Hazard for the US East Coast. Geophys Res Lett (in preparation).

ten Brink, U, Twichell D, Geist E, Chaytor J, Locat J, Lee H, Buczkowski B, Barkan R, Solow A, Andrews B, Parsons T, Lynett P, Lin J, and M Sansoucy (2008). Evaluation of tsunami sources with the potential to impact the U.S. Atlantic and Gulf coasts. USGS Administrative report to the U.S. Nuclear Regulatory Commission, 300 pp.

ten Brink US, Lee HJ, Geist EL and D Twichell (2009a) Assessment of tsunami hazard to the U.S. East Coast using relationships between submarine landslides and earthquakes. Mar Geol, 264:65-73.

ten Brink US, Barkan R, Andrews BD and JD Chaytor (2009b) Size distributions and failure initiation of submarine and subaerial landslides. Earth Planetary Sci Lett, 287:31-42.

ten Brink US, Chaytor JD, Geist EL, Brothers DS and BD Andrews (2014) Assessment of tsunami hazard to the U.S. Atlantic margin. Mar Geol, 353:31-54.

Towns J, Cockerill T, Dahan M, Foster I, Gaither K, Grimshaw A, Hazlewood V, Lathrop S, Lifka D, Peterson GD, Roskies R, Scott JR and N Wilkins-Diehr (2014). XSEDE: Accelerating Scientific Discovery. Computing in Science and Engineering 16(5):62-74. doi:10.1109/MCSE.2014.80.

Watts P, Grilli ST, Tappin DR and G Fryer (2005). Tsunami generation by submarine mass failure, II: Predictive equations and case studies. J Waterw Port Coast Oc Engng, 131(6):298-310.

A SMF geometry and slump law of motion

For rigid slumps, kinematics is specified based on the analytical laws developed by Grilli and Watts (1999, 2005); Watts et al. (2005). Additionally, as in Enet and Grilli (2007), the SMF geometry is idealized as having a "Quasi-Gaussian" shape (below seafloor) of elevation $\zeta(x,y)$, whose steepness is controlled by a shape parameter ε (here $\varepsilon = 0.717$), and elliptical footprint of downslope length b, width w, and maximum thickness T defined as (Fig. 13),

$$\zeta(x,y) = \frac{T}{1-\varepsilon}\max\{0, \operatorname{sech}(k_b\xi)\operatorname{sech}(k_w\chi) - \varepsilon\} \tag{1}$$

where (ξ, χ) are the local downslope and spanwise horizontal coordinates, rotated in the direction of SMF motion θ, and $k_b = 2C/b$, $k_w = 2C/w$, with $C = \operatorname{acosh}(1/\varepsilon)$. With this geometry and parameters, the SMF volume is given by,

$$V_s = bwT\frac{I_2}{C^2}\left(\frac{\frac{I_1}{I_2}-\varepsilon}{1-\varepsilon}\right) \quad \text{with} \quad I_{1;2} = \int_0^C f(\mu)\,\mathrm{d}\mu; g(\mu)\,\mathrm{d}\mu \tag{2}$$

and,

$$f(\mu) = \text{sech}\,\mu \, \text{atan}(\sinh g(\mu)) \quad , \quad g(\mu) = \text{acosh}\left(\frac{\text{sech}\,\mu}{\varepsilon}\right) \tag{3}$$

[Note that Eqs. (2) and (3) have been corrected and are different from those reported in earlier papers (e.g., Enet and Grilli (2007); Grilli et al. (2015)), which resulted from a mistake in the volume calculation.] For the specified ε, we find, $C = 0.8616$, $I_1 = 0.4804$, $I_2 = 0.5672$, and $V_s = 0.3508\,bwT$.

Earlier modeling work (Locat et al., 2009) indicates that, during its tsunamigenic period of motion, the Currituck SMF achieved a relatively small maximum displacement (runout) $S_f < b$ in its main direction of motion down the slope, over an unknown time of motion t_f. The combination of rigid block SMF and small displacement parallel to the slope supports modeling the SMF kinematics as a rigid slump or a deforming slide with moderate deformation achieving a similar runout over the same time. In either cases, one can assume a constant basal friction (i.e., slide to substrate friction) and negligible hydrodynamic drag (Grilli and Watts, 2005). This type of rigid-body motion kinematics was investigated in earlier work (see above-listed references), leading for the slump to a pendulum-like center of mass motion $S(t)$ parallel to the local mean slope of angle α. Here, we use this simple law of motion for rigid slumps, which reads,

$$S(t) = S_0\left(1 - \cos\frac{t}{t_0}\right) \quad \text{for} \quad 0 \le t \le t_f \tag{4}$$

with $S_0 = S_f/2$ and $t_0 = t_f/\pi$, and $S = S_f$ for $t > t_f$ (assuming SMF triggering occurs at $t = 0$).

At $t = 0$, the SMF elevation is specified below the current seafloor bathymetry $h_0(x, y)$. Given the SMF initial center of mass location (x_0, y_0) in global axes (x, y) (i.e., coordinates of the center of the elliptical footprint) and azimuth angle of SMF motion θ, we define the coordinate transformation to the local SMF slope-parallel coordinate system (ξ, χ) (Fig. 13) as,

$$\begin{aligned} \xi &= (x - x_o)\cos\theta - (y - y_0)\sin\theta - S(t)\cos\alpha \\ \chi &= (x - x_o)\sin\theta + (y - y_0)\cos\theta \end{aligned} \tag{5}$$

with $S(t)$ given by Eq. (4).

Then, assuming $\sin\alpha \simeq 0$ for small slopes, the instantaneous seafloor depth above the SMF is given by,

$$h(x, y, t) = h_0(x, y) + \zeta\{\xi(x, y, t), \chi(x, y, t)\} - \zeta\{\xi(x, y, 0), \chi(x, y, 0)\} \tag{6}$$

with $\Delta h = h - h_0$. The seafloor motion described by Eq. (6) is similar to a translation parallel to the average slope of part of the seabed, over the actual bathymetry. The vertical seafloor velocity (used in NHWAVE as a bottom boundary condition) is computed as,

$$\frac{dh}{dt}(x, y, t) = \frac{d\zeta}{dt}\{\xi(x, y, S(t)), \chi(x, y, t)\} \tag{7}$$

33
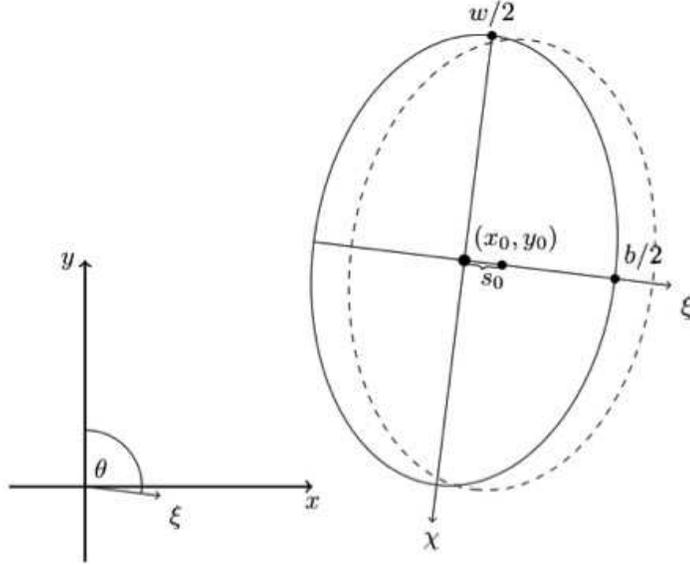
Figure 13: Geometric parameterization of a SMF initially centered at (x_0, y_0) moving in direction ξ, with an azimuth angle θ from North and center of mass motion $S(t)$ measured parallel to the mean local slope of angle α; (x, y) denote the longitudinal and latitudinal horizontal directions, respectively.

which can be easily derived from Eqs. (1) to (6) as,

$$\frac{\mathrm{d}h}{\mathrm{d}t}(x, y, t) = k_b \cos \alpha \left(\zeta + \frac{\varepsilon T}{1 - \varepsilon} \right) U \tanh(k_b \xi) \quad \text{with} \quad U(t) = \frac{\mathrm{d}S}{\mathrm{d}t} = U_{max} \sin \frac{t}{t_0} \quad (8)$$

the slump velocity obtained from Eq. (4), with $U_{max} = S_0/t_0$ the maximum velocity. Similarly, the slump acceleration is found as,

$$A(t) = \frac{\mathrm{d}^2 S}{\mathrm{d}t^2} = A_0 \cos \frac{t}{t_0} \quad \text{with} \quad A_0 = \frac{S_0}{t_0^2} \quad (9)$$

the initial acceleration.

For rigid slumps, hydrodynamic drag can be neglected due to low velocity and small amplitude of motion, and inertia includes both the SMF mass $M_s = \rho_s V_s$, with ρ_s denoting the sediment bulk density, and the specific density being defined as $\gamma = \rho_s/\rho_w$, with ρ_w the water density, and an added mass $\Delta M_s = C_M \rho_w V_s$, defined by way of an added mass coefficient C_M. Assuming a constant basal friction, a nearly circular rupture surface of radius R, and a small angular displacement $\Delta\Phi$, Grilli and Watts (2005) derived the characteristic distance and time of motion for rigid slumps as,

$$S_0 = \frac{R \Delta \Phi}{2} \quad \text{and} \quad t_0 = \sqrt{\frac{R}{g} \frac{\gamma + C_M}{\gamma - 1}} \quad \text{with} \quad R \simeq \frac{b^2}{8T} \quad (10)$$

with g denoting the gravitational acceleration. The last equation (10), proposed by Watts et al. (2005), is a semi-empirical relationship to estimate the radius of slump motion as a function of slump downslope length and maximum thickness.

34